

Fast Synchronization of FSK Signals

Konstantinos M. Konstantinidis

A thesis submitted in partial fulfillment for the
Diploma

in the

School of Electrical and Computer Engineering
Technical University of Crete

Supervisor

Assoc. Prof. George N. Karystinos

Committee members:

Assoc. Prof. Aggelos Bletsas

Assist. Prof. Daphne Manousaki

December 2016

Contents

1	Introduction	7
2	Detection in OQPSK	9
2.1	Signal model	9
2.2	The likelihood function	10
2.3	Likelihood maximization	14
2.4	Likelihood and sequence properties	15
2.5	Detection of sequence changes	18
2.6	Noncoherent detection algorithm and results	22
3	Detection in FSK	27
3.1	Signal model	27
3.2	The likelihood function	27
3.3	Likelihood maximization	28
3.4	Detection of sequence changes	29
3.5	Likelihood properties, noncoherent detection algorithm and results	30
3.6	Coherent detection	33
	OQPSK Appendix	37
A.1	Likelihood derivation	37
A.2	CLF general form	37
A.3	Limits of the likelihood	38
A.4	Mackenthun's maximization with respect to angle	39
A.5	CLF maximization equivalent problem	39
A.6	CLF periodicity proof	40
A.7	Equivalent correlation of angles in the frequency domain	40
A.8	CLF simplified form	41
A.9	2D Parseval's theorem	41
A.10	2D frequency shifting property	42
	FSK Appendix	43
B.1	Likelihood form	43

B.2	Maximization algorithm's input	44
B.3	Angles' correlation case 1	44
B.4	Angles' correlation case 2	45
B.5	Constant likelihood	46
B.6	Alternative likelihood	47
B.7	Alternative likelihood derivative	47
B.8	Conditional PDF of received sample (hypothesis testing)	48
B.9	Maximum likelihood decision rule	49
B.10	Limits of the likelihood	49

Bibliography		51
---------------------	--	-----------

Abstract

In this diploma thesis, we address the problem of noncoherent synchronization, channel estimation, and detection for offset quadrature phase-shift keying (OQPSK) and binary frequency-shift keying (BFSK) modulations. We develop a gradient-descent algorithm which exploits some characteristics of the concentrated likelihood function (CLF) of the time delay as well as some observations about the transmitted sequences and performs noncoherent synchronization, channel estimation, and detection for the aforementioned types of modulation. The proposed algorithm is based on the efficient noncoherent detection of the transmitted symbols, under channel and timing uncertainty. The development of our algorithm is based on the maximum-likelihood (ML) criterion and utilizes state-of-the-art noncoherent detection techniques from the literature. After we reproduce the results of a recent work on joint noncoherent synchronization, channel estimation, and detection for OQPSK, we design an algorithm that concentrates on the data detection problem and is applicable for both OQPSK and BFSK. We are mainly interested in the transmitted sequence but a clock estimate is obtained as byproduct. The latter is achieved by converting the likelihood function to a form that depends only on the estimates of the transmitted sequences and the actual channel delay. The method used involves the first-order derivative of the likelihood with respect to the delay as well as some useful properties of the estimated sequences.

Introduction

In this diploma thesis, we have addressed the problem of noncoherent detection in OQPSK and BFSK modulations. When implemented exhaustively, by searching among all possible sequences, detection demonstrates exponential complexity (in the sequence length). In the following text, we propose a gradient descent algorithm which exploits some characteristics of the CLF of the time delay as well as some observations about the sequences and performs detection for the aforementioned types of modulation. The following work follows the novel work that our group has done in non-coherent FSK detection [1]. The difference between this paper and my thesis is that in the former the clock parameter is considered as known at the receiver while I have considered it as unknown.

Phase-shift keying (PSK) is a digital modulation scheme that conveys data by changing (modulating) the phase of a reference signal (the carrier wave). The modulation is impressed by varying the sine and cosine inputs at a precise time. It is widely used for wireless Local area networks (LANs) and Radio-frequency identification (RFID) communication. Any digital modulation scheme uses a finite number of distinct signals to represent digital data. PSK uses a finite number of phases, each assigned a unique pattern of binary digits. Usually, each phase encodes an equal number of bits. Each pattern of bits forms the symbol that is represented by the particular phase.

Frequency-shift keying (FSK) is a frequency modulation scheme in which digital information is transmitted through discrete frequency changes of a carrier signal. The technology is used for low-rate communication systems in small Signal-to-noise ratio (SNR) environments (power-limited regime) such as amateur radio, caller ID and emergency broadcasts. The simplest FSK is binary FSK (BFSK). BFSK uses a pair of discrete frequencies to transmit binary (± 1 s) information. With this scheme, the "+1" is called the mark frequency and the "-1" is called the space frequency.

In this study, we propose an efficient algorithm in order to obtain estimates of the transmitted symbols. The derivation is based on the ML criterion, and utilizes a very efficient algorithm for the detection of differentially encoded symbols already described in literature. I initially examined a paper which proposes an algorithm for joint carrier phase and timing estimation for OQPSK[2], reproduced its basic results and designed an algorithm for blind synchronization and detection for OQPSK and BFSK modulations. The latter is achieved by bringing the likelihood function to a form that depends only on the estimates of the transmitted sequences ($\hat{\mathbf{a}}$ (in-phase) and $\hat{\mathbf{b}}$ (quadrature) for OQPSK and $\hat{\mathbf{x}}$ for BFSK) and the actual channel delay ($\tilde{\tau}$). We are mainly interested in the transmitted sequence but a clock estimate is obtained as byproduct. The method used involves the first-order derivative of the likelihood with respect to the

delay as well as some useful properties of the estimated sequences.

Notation conventions: Bold upper-case and lower-case symbols will denote matrices and vectors, respectively, while lower-case non bold letters will be used for scalars and other variables. The symbol $(\cdot)^*$ will stand for the complex conjugation operation and the $(\cdot)^T$ for the transpose operator whereas the complex Gaussian distribution with mean μ and variance σ^2 is denoted by $\mathcal{CN}(\mu, \sigma^2)$. The real part of a complex number will be represented by $\Re\{\cdot\}$ and the imaginary part by $\Im\{\cdot\}$. The notation A. x will denote the x -th section of the appendix at the end of the document. Finally, the symbol $(\cdot)^H$ will be used for the Hermitian of a matrix.

Detection in OQPSK

2.1 Signal model

The constellation of the modulation represents the complex information symbols that correspond to the complex envelopes of the four possible signals to be transmitted. The signalling pulse has unary energy ($Eg = 1$) adhering to the orthonormality criterion. This quantity gives us the energy required to transmit the in-phase or quadrature component of the signal in passband. The OQPSK constellation is a special case of the QPSK modulation where neighboring symbols differ by $\pm\pi/2$ and consecutively transmitted symbols can only differ by $\pm\pi/2$ in terms of phase and changes of phase by $\pm\pi$ are not feasible. In general, we can start by an arbitrary phase θ_0 and then the rest of the M -PSK symbols are defined according to this phase

$$x_i \in \left\{ e^{+j\theta_0}, e^{+j\frac{2\pi}{M}+j\theta_0}, e^{+j2\frac{2\pi}{M}+j\theta_0}, \dots, e^{+j(M-1)\frac{2\pi}{M}+j\theta_0} \right\} \quad (2.1)$$

All of the points are placed on the circumference of a circle in the complex plane around the point $(0, 0)$. The constellation that we used is represented in Fig. 2.1, where the dotted lines represent the feasible shift changes across consecutive symbols.

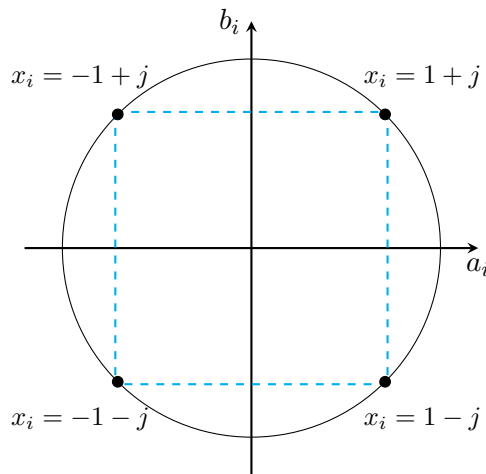


Figure 2.1: OQPSK constellation.

The signal in complex form is

$$s(t) = \sum_i a_i g(t - iT) + j \sum_i b_i g(t - T/2 - iT) \quad (2.2)$$

The signalling pulse is a real-valued function and more precisely a square-root-raised-cosine (SRRC) pulse that is widely used in digital communications since its shifts by multiples of its parameter T constitute an orthonormal set. It is defined as

$$g(t) = \begin{cases} \frac{4\alpha}{\pi\sqrt{T}} \frac{\cos((1+\alpha)\frac{\pi t}{T}) + \frac{\sin((1-\alpha)\frac{\pi t}{T})}{\frac{4\alpha t}{T}}}{1 - (\frac{4\alpha t}{T})^2}, & t \in [0, D_g T) \\ 0, & \text{otherwise} \end{cases} \quad (2.3)$$

where $T > 0$, $a > 0$, $D_g \in \mathbb{N}$ are a parameter, the roll-off factor and the duration in number of periods, respectively.

Returning back to equation (2.2), $T > 0$ symbolizes the symbol period while the vectors $\mathbf{a} = \{a_i\}$ and $\mathbf{b} = \{b_i\}$ are the in-phase and quadrature symbols, accordingly. The symbols are independent, identically distributed and are equiprobably matched to the values $\{\pm 1\}$. We should also note that the receiver has memory on the grounds that the modulated signal depends on a finite number of previous information symbols, at any given time.

The channel adds complex Gaussian white noise $w(t)$ with independent real and imaginary parts and the model considers a flat-fading channel leading to a received waveform of

$$r(t) = \tilde{h} e^{j\tilde{\theta}} s(t - \tilde{\tau}) + n(t) \quad (2.4)$$

after downconversion where $\tilde{h} > 0$, $\tilde{\theta} \in \mathbb{R}$ and $\tilde{\tau} \in \mathbb{R}$ denote the attenuation, the phase change and the actual time delay that the use of the channel entails. These parameters can be considered constant in the course of time by making the assumption that the time in which the impulse response of the channel can change is much longer than the observation interval across which the transmission occurs.

The need to estimate both the carrier phase $\tilde{\theta}$ and the propagation delay $\tilde{\tau}$ emerges from the fact that the oscillator which produces the carrier signal for demodulation at the receiver is generally not synchronous in phase with that at the transmitter. Furthermore, the two oscillators may be drifting slowly with time, perhaps in different directions. Consequently, the received carrier phase is not only dependent on the time delay $\tilde{\tau}$. Furthermore, the precision to which one must synchronize in time for the purpose of demodulating the received signal depends on the symbol interval T .

2.2 The likelihood function

All of the parameters introduced in (2.4) are unknown to the receiver and must be estimated. In this work, we primarily focus on the synchronization of the channel and the sequence detection by adopting the ML criterion. We observe the received signal $r(t)$ in the interval $[0, T_0)$, where $T_0 = L_0 T$ and $L_0 \in \mathbb{N}$.

The equivalent expression for the signal $s(t)$ can be obtained by its baseband complex envelope, say $s_l(t)$ as

$$s(t) = \Re \left\{ s_l(t) e^{j2\pi f_c t} \right\} \quad (2.5)$$

where f_c is the carrier frequency.

Equivalently, the received signal is

$$r(t) = \Re \left\{ [\tilde{h}s_l(t - \tilde{\tau})e^{j\tilde{\theta}} + z(t)]e^{j2\pi f_c t} \right\} \quad (2.6)$$

where $z(t)$ is the low-pass equivalent signal of the noise. All of the parameters need to be estimated for demodulation and coherent detection. Consequently, the received signal is a function of these parameters

$$r(t) = \tilde{h}e^{j\tilde{\theta}}s(t - \tilde{\tau}) + n(t) = s(t; \tilde{h}, \tilde{\theta}, \tilde{\tau}) + n(t) = s(t; \boldsymbol{\theta}) + n(t) \quad (2.7)$$

where all of the parameters have been incorporated in the parameter vector $\boldsymbol{\theta}$. In the ML criterion, the signal parameter vector $\boldsymbol{\theta}$ is treated as deterministic but unknown. From the Gram-Schmidt procedure, we derive an orthonormal basis for $s(t)$ with N orthonormal functions $\{\phi_n(t)\}$ and the received vector can be approximated by a vector of coefficients $\mathbf{r} = [r_1 \ r_2 \ \dots \ r_N]$. The ML estimate of $\boldsymbol{\theta}$ maximizes the PDF $p(\mathbf{r}|\boldsymbol{\theta})$ and this criterion demands an observation interval $T_0 \geq T$. Because of the Gaussian zero-mean noise and the fact that the elements of \mathbf{r} are iid, the PDF can be written as

$$p(\mathbf{r}|\boldsymbol{\theta}) = \prod_{n=1}^N p(r_n|\boldsymbol{\theta}) = \prod_{n=1}^N \frac{1}{\sqrt{2\pi}\sigma} \exp \left\{ -\frac{[r_n - s_n(\boldsymbol{\theta})]^2}{2\sigma^2} \right\} \quad (2.8)$$

$$= \left(\frac{1}{\sqrt{2\pi}\sigma} \right)^N \exp \left\{ -\sum_{n=1}^N \frac{[r_n - s_n(\boldsymbol{\theta})]^2}{2\sigma^2} \right\} \quad (2.9)$$

where

$$r_n = \int_{T_0} r(t)\phi_n(t)dt \quad (2.10)$$

$$s_n(\boldsymbol{\theta}) = \int_{T_0} s(t; \boldsymbol{\theta})\phi_n(t)dt \quad (2.11)$$

By the expansion we have that

$$r(t) = \sum_{n=1}^N r_n\phi_n(t) \quad (2.12)$$

and

$$s(t; \boldsymbol{\theta}) = \sum_{n=1}^N s_n(\boldsymbol{\theta})\phi_n(t) \quad (2.13)$$

So

$$\frac{1}{N_0} \int_{T_0} [r(t) - s(t; \boldsymbol{\theta})]^2 dt = \frac{1}{2\sigma^2} \int_{T_0} \sum_{n=1}^N [r_n - s_n(\boldsymbol{\theta})]^2 dt \quad (2.14)$$

and the proof is in A.1.

Plugging (2.14) into (2.9) yields

$$p(\mathbf{r}|\boldsymbol{\theta}) = \left(\frac{1}{\sqrt{2\pi}\sigma} \right)^N \exp \left\{ -\frac{1}{N_0} \int_{T_0} [r(t) - s(t; \boldsymbol{\theta})]^2 dt \right\} \quad (2.15)$$

The objective now transforms into maximizing $p(\mathbf{r}|\boldsymbol{\theta})$ but since the first term is independent of the parameters the likelihood becomes

$$\Lambda(\boldsymbol{\theta}) = \exp \left\{ -\frac{1}{N_0} \int_{T_0} [r(t) - s(t; \boldsymbol{\theta})]^2 dt \right\} \quad (2.16)$$

The maximization leads to the following derivation

$$\operatorname{argmax}_{\boldsymbol{\theta}} \Lambda(\boldsymbol{\theta}) = \operatorname{argmax}_{\boldsymbol{\theta}} -\frac{1}{N_0} \int_{T_0} |r(t) - s(t; \boldsymbol{\theta})|^2 dt = \operatorname{argmin}_{\boldsymbol{\theta}} \int_{T_0} |r(t) - s(t; \boldsymbol{\theta})|^2 dt \quad (2.17)$$

$$= \operatorname{argmin}_{\boldsymbol{\theta}} \int_{T_0} |r(t)|^2 + |s(t; \boldsymbol{\theta})|^2 - 2\Re\{r(t)s^*(t; \boldsymbol{\theta})\} dt \quad (2.18)$$

$$= \operatorname{argmax}_{\boldsymbol{\theta}} \int_{T_0} 2\Re\{r(t)s^*(t; \boldsymbol{\theta})\} - |s(t; \boldsymbol{\theta})|^2 dt \quad (2.19)$$

where in the last equality we have ignored the term which is independent of the parameter. By the expressions in (2.7) and (2.19) we can conclude that the likelihood function in our case is

$$\Lambda(\mathbf{a}, \mathbf{b}, h, \theta, \tau) = 2h \left| \int_0^{T_0} r(t)s^*(t - \tau) dt \right| \cos(-(\theta - \vartheta(\mathbf{a}, \mathbf{b}, \tau))) - h^2 \int_0^{T_0} |s(t - \tau)|^2 dt \quad (2.20)$$

where

$$\vartheta(\mathbf{a}, \mathbf{b}, \tau) = \arg \left\{ \int_0^{T_0} r(t)s^*(t - \tau) dt \right\} \quad (2.21)$$

and the proof is shown in A.2.

The fact that \mathbf{a} , \mathbf{b} , h , θ and τ are all independent allows to maximize this expression consecutively with respect to each of its variables. From (2.20), it is apparent that the second term is irrelevant to the maximization with respect to θ and that the optimal estimate is achieved for

$$\hat{\theta} = \vartheta(\mathbf{a}, \mathbf{b}, \tau) \quad (2.22)$$

Plugging (2.22) to (2.20) brings the likelihood to the form

$$\Lambda(\mathbf{a}, \mathbf{b}, h, \tau) = 2h \left| \int_0^{T_0} r(t)s^*(t - \tau) dt \right| - h^2 \int_0^{T_0} |s(t - \tau)|^2 dt \quad (2.23)$$

Setting the first partial derivative of the above function, with respect to h , to zero yields

$$\frac{\partial \Lambda(\mathbf{a}, \mathbf{b}, h, \tau)}{\partial h} = 2 \left| \int_0^{T_0} r(t)s^*(t - \tau) dt \right| - 2h \int_0^{T_0} |s(t - \tau)|^2 dt = 0 \quad (2.24)$$

$$\Rightarrow \hat{h} = \frac{\left| \int_0^{T_0} r(t)s^*(t - \tau) dt \right|}{\int_0^{T_0} |s(t - \tau)|^2 dt} \quad (2.25)$$

and substituting this form into the expression of (2.23) we get

$$\Lambda(\mathbf{a}, \mathbf{b}, \tau) = \frac{\left| \int_0^{T_0} r(t)s^*(t - \tau) dt \right|^2}{\int_0^{T_0} |s(t - \tau)|^2 dt} \quad (2.26)$$

At this point we need to eliminate the denominator for the maximization. Its value depends on all of the parameters but it can be proven that this dependence becomes smaller as the observation interval T_0 increases and simulations have exhibited that the absolute value of this integral decreases when the excess bandwidth of the SRRC pulse increases[2]. For that the roll-off factor of the pulse can be adjusted because its bandwidth equals exactly $(1 + a)/(2T)$. Dropping the integral, the function reads:

$$\Lambda(\mathbf{a}, \mathbf{b}, \tau) = \left| \int_0^{T_0} r(t) s^*(t - \tau) dt \right|^2 \quad (2.27)$$

Using (2.2) in (2.27) yields

$$\Lambda(\mathbf{a}, \mathbf{b}, \tau) = \left| \int_0^{T_0} r(t) \left[\sum_i a_i g(t - \tau - iT) - j \sum_i b_i g(t - \tau - T/2 - iT) \right] dt \right|^2 \quad (2.28)$$

$$= \left| \sum_i a_i \int_0^{T_0} r(t) g(t - \tau - iT) dt - j \sum_i b_i \int_0^{T_0} r(t) g(t - \tau - T/2 - iT) dt \right|^2 \quad (2.29)$$

$$= \left| \sum_{i=-D_g}^{L_0-1} a_i X_i(\tau) - j \sum_{i=-D_g}^{L_0-1} b_i X_{i+1/2}(\tau) \right|^2 \quad (2.30)$$

where

$$X_i(\tau) = \int_0^{T_0} r(t) g(t - \tau - iT) dt \quad (2.31)$$

and

$$X_{i+1/2}(\tau) = \int_0^{T_0} r(t) g(t - \tau - T/2 - iT) dt \quad (2.32)$$

The fact that the summations in the likelihood function can be restricted to $L_0 + D_g$ terms as can be seen in (2.30) is proved in A.3. The maximization of (2.30) has exponential complexity to the sequence length when executed exhaustively, but the Mackenthun's algorithm in [5] deals with this task in polynomial time. The algorithm as well as the proof that it corresponds to our problem are given in the next section.

Therefore the objective is to find the M-PSK symbols defined in (2.1) that maximize the quantity

$$\left| \sum_{k=0}^{2(L_0+D_g)-1} c_k^* y_k \right|^2 \quad (2.33)$$

with $y_k \in \mathbb{C}, \forall k \in \{0, 1, \dots, 2(L_0 + D_g) - 1\}$. The variables in (2.33) are defined as

$$c_k = e^{j\phi_k}, \quad \phi_k \in \{0, 2\pi/M, \dots, 2\pi(M-1)/M\} \quad (2.34)$$

$$c_{2i} = a_{-D_g+i} \quad (2.35)$$

$$c_{2i+1} = b_{-D_g+i}$$

and

$$y_{2i} = X_{-D_g+i}(\tau) \quad (2.36)$$

$$y_{2i+1} = -j X_{-D_g+i+1/2}(\tau)$$

for $i \in \{0, 1, \dots, L_0 + D_g - 1\}$ and the symbols and $M = 2$. The optimal sequences returned by the algorithm are substituted in (2.30) yielding the final form of the likelihood as a function of only the clock which is

$$\Lambda(\tau) = \left| \sum_{i=-D_g}^{L_0-1} \hat{a}_i(\tau) X_i(\tau) - j \sum_{i=-D_g}^{L_0-1} \hat{b}_i(\tau) X_{i+1/2}(\tau) \right|^2 \quad (2.37)$$

so that both sequences are function of τ .

2.3 Likelihood maximization

The objective of the algorithm is to find the binary sequence $\mathbf{d} \in \{\pm 1\}^{N+1}$ that for a given complex vector $\mathbf{y} \in \mathbb{C}^{N+1}$ maximizes the quantity $|\mathbf{d}^T \mathbf{y}|$ so that

$$\begin{aligned} \max_{\mathbf{d} \in \{\pm 1\}^{N+1}} |\mathbf{d}^T \mathbf{y}| &= \max_{\mathbf{d} \in \{\pm 1\}^{N+1}} |d_0 y_0 + d_1 y_1 + \dots + d_N y_N| \quad (2.38) \\ &= \max_{\phi \in [0, 2\pi)} \max_{\mathbf{d} \in \{\pm 1\}^{N+1}} \left\{ d_0 \Re \left\{ e^{-j\phi} y_0 \right\} + d_1 \Re \left\{ e^{-j\phi} y_1 \right\} + \dots \right. \\ &\quad \left. \dots + d_N \Re \left\{ e^{-j\phi} y_N \right\} \right\} \quad (2.39) \end{aligned}$$

For a proof you can see A.4. At this point, we can perform independent maximizations for each term of the inner maximization in (2.39) for all $d_n, n \in \{0, 1, \dots, N\}$ as

$$\hat{d}_n = \operatorname{argmax}_{d_n \in \{\pm 1\}} d_n \Re \left\{ e^{-j\phi} y_n \right\} \Leftrightarrow \Re \left\{ e^{-j\phi} y_n \right\} \underset{\hat{d}_n = -1}{\overset{\hat{d}_n = +1}{\geq}} 0 \quad (2.40)$$

$$\Leftrightarrow |y_n| \Re \left\{ e^{-j(\phi - \vartheta_n)} \right\} \underset{\hat{d}_n = -1}{\overset{\hat{d}_n = +1}{\geq}} 0 \quad (2.41)$$

$$\Leftrightarrow |y_n| \cos(\phi - \vartheta_n) \underset{\hat{d}_n = -1}{\overset{\hat{d}_n = +1}{\geq}} 0 \quad (2.42)$$

$$\Leftrightarrow \cos(\phi - \vartheta_n) \underset{\hat{d}_n = -1}{\overset{\hat{d}_n = +1}{\geq}} 0 \quad (2.43)$$

where $\vartheta_n = \arg \{y_n\}$. The decision for \hat{d}_n according to (2.43) changes at the following set of points

$$\phi = \pm \frac{\pi}{2} + \vartheta_n \pmod{2\pi} \quad (2.44)$$

for $\phi \in [0, 2\pi)$. The relation (2.44) provides $2(N + 1)$ points but we can observe that for any value of n the two angles of (2.44) differ by π so that for any $\phi \in [0, \pi)$ the sequences obtained at ϕ and $\phi + \pi$ are the opposite leading to the same metric in (2.38) and the search can be restricted to any semicircle so without loss of generality $\phi \in [0, \pi)$. The angle at which the n -th decision changes is

$$\phi_n = \frac{\pi}{2} + \vartheta_n \pmod{\pi}, \quad n \in \{0, 1, \dots, N\} \quad (2.45)$$

Subsequently we sort the $N + 1$ points through

$$(\theta_0, \theta_1, \dots, \theta_N) = \operatorname{sort}(\phi_0, \phi_1, \dots, \phi_N) \quad (2.46)$$

which is necessary in order to define the intervals across which the decision $\hat{\mathbf{d}}$ remains constant are

$$C_0 = (\theta_*, \theta_0), C_1 = (\theta_0, \theta_1), \dots, C_N = (\theta_{N-1}, \theta_N) \quad (2.47)$$

The interval (θ_N, π) can be ignored due to the fact that all of \hat{d}_n s would have changed compared to those of C_0 producing the opposite sequence¹. Equivalently, we could have ignored C_0 . Our goal is to detect the vectors $\hat{\mathbf{d}}_0, \hat{\mathbf{d}}_1, \dots, \hat{\mathbf{d}}_N$ associated with the above intervals. The key is that the sequences of the adjacent intervals $\hat{\mathbf{d}}_n$ and $\hat{\mathbf{d}}_{n+1}$ differ only at the n -th element and specifically at the k -th multiplier for $\theta_n = \phi_k$ so that

$$\hat{d}_n = \begin{cases} \hat{d}_n, & \phi \in C_k, k \leq n \\ -\hat{d}_n, & \phi \in C_k, k > n \end{cases} \quad (2.48)$$

The algorithm exploits this property by visiting the angles $\theta_0, \theta_1, \dots, \theta_N$ consecutively, producing the sequences and returning that with the maximum metric.

At each point θ_i , the new sequence is produced with constant complexity by inverting \hat{d}_i and its metric is also calculated at a constant computational cost. The pseudocode is illustrated in Fig. 2.2 and the upper limit of its complexity is that of the sorting operation which is $\mathcal{O}((N+1) \log_2(N+1)) \approx \mathcal{O}(N \log N)$.

We need to prove that the problem introduced in (2.33) is equivalent to the maximization of (2.30). From (2.33) we have that

$$\left| \sum_{k=0}^{2(L_0+D_g)-1} c_k^* y_k \right|^2 = \left| \sum_{i=-D_g}^{L_0-1} a_i X_i(\tau) - j \sum_{i=-D_g}^{L_0-1} b_i X_{i+1/2}(\tau) \right|^2 \quad (2.49)$$

Resort to A.5 for a proof. The channel uses M -PSK modulation for $M = 2$ and from (2.34)

$$c_k = e^{j\phi_k}, \quad \phi_k \in \{0, \pi\} \quad (2.50)$$

$$= \cos \phi_k + j \sin \phi_k, \quad \phi_k \in \{0, \pi\} \quad (2.51)$$

$$= \begin{cases} 1, & \phi_k = 0 \\ -1, & \phi_k = \pi \end{cases} \quad (2.52)$$

that renders c_k s binary taking on the values $\{\pm 1\}$ just like the sequences of the OQPSK modulation **a** and **b**.

2.4 Likelihood and sequence properties

Typical shapes of the CLF in (2.37) are provided in Fig. 2.3 and were normalized to their maximum values. This figure corresponds to one realization of the experiment. The value of $\tilde{\tau}$ clearly affects the matched filter responses of (2.31) and (2.32) leading to different shapes. The roll-off factor of the SRRC used is $\alpha = 0.1$. Also an observation length of $L_0 = 100$ symbols, signalling pulse duration of $D_g = 16$ periods, and a signal-to-noise ratio of 30dB have been utilized. As expected, the maximum value of $\Lambda(\tau)$ is achieved at the actual channel delay $\tilde{\tau}$. The difference between the values of the likelihood for values of τ that are $T/2$ away is observed to be negligible as the observation interval increases. The value of the phase change θ used is arbitrary.

¹ θ_* is the initial point of search equal to $\theta_* = \frac{\theta_N - \pi}{2} < 0$ that is used if $\theta_0 = 0$ to resolve the ambiguity that would arise if we estimate the sequence exactly at a point of change as shown by (2.43).

Algorithm 1 Optimal Noncoherent Antipodal Decoding in Time $\mathcal{O}(N \log N)$

Input: y_0, y_1, \dots, y_N

```

1: for  $n = 0 : N$  do
2:    $\phi_n := \frac{\pi}{2} + \vartheta_n \pmod{\pi}$ 
3: end for
4:  $(\theta_0, \theta_1, \dots, \theta_N) = \text{sort}(\phi_0, \phi_1, \dots, \phi_N)$ 
5: if  $\theta_0 > 0$  then
6:    $\theta^* := 0$ 
7: else
8:    $\theta^* = \frac{\theta_N - \pi}{2}$ 
9: end if
10: for  $n = 0 : N$  do
11:    $\hat{d}_n = \text{sign}(\Re\{e^{-j\theta^*} y_n\})$ 
12: end for
13:  $\hat{\mathbf{d}}^{\text{ML}} := \hat{\mathbf{d}}$ 
14:  $\text{value}_{\hat{\mathbf{d}}} := \hat{d}_0 y_0 + \hat{d}_1 y_1 + \dots + \hat{d}_N y_N$ 
15:  $\text{ML\_value} := |\text{value}_{\hat{\mathbf{d}}}|$ 
16: for  $i = 0 : N - 1$  do
17:   let  $n$  be the index for which  $\theta_i = \phi_n$  at line 4
18:    $\text{value}_{\hat{\mathbf{d}}} := \text{value}_{\hat{\mathbf{d}}} - 2\hat{d}_n y_n$ 
19:    $\hat{d}_n = -\hat{d}_n$ 
20:   if  $|\text{value}_{\hat{\mathbf{d}}}| > \text{ML\_value}$  then
21:      $\text{ML\_value} := |\text{value}_{\hat{\mathbf{d}}}|$ 
22:      $\hat{\mathbf{d}}^{\text{ML}} := \hat{\mathbf{d}}$ 
23:   end if
24: end for

```

Figure 2.2: Optimal noncoherent sequence detection algorithm in time $\mathcal{O}(N \log N)$.

An SNR value of x is obtained by setting

$$h = \sqrt{\frac{E_s}{N_0}} = \sqrt{10^{\text{SNR}_{dB}/10}} \quad (2.53)$$

where E_s and N_0 are the power of the signal and the noise respectively. At each point the optimal sequence is estimated by the proposed algorithm in Chapter 2.3 and its metric is evaluated. We observe that this function is periodic with a period of $T/2$. Indeed, the OQPSK model demands that $\hat{a}_i(\tau + T/2) = -\hat{b}_i(\tau)$ and $\hat{b}_i(\tau + T/2) = -\hat{a}_{i+1}(\tau)$ because the in-phase and quadrature parts change independently and cannot change concurrently. By (2.37) and setting

$$Y(\tau) = \sum_{i=-D_g}^{L_0-1} \hat{a}_i(\tau) X_i(\tau) - j \sum_{i=-D_g}^{L_0-1} \hat{b}_i(\tau) X_{i+1/2}(\tau) \quad (2.54)$$

it follows that

$$\Lambda(\tau + T/2) \approx |Y(\tau)|^2 = \Lambda(\tau) \quad (2.55)$$

The proof can be found at A.6. Another notice that attests to the periodicity of the CLF is the fact that simulations show that if the winning sequence changes at $\tau = \tau_1$, then there is also a sequence change in

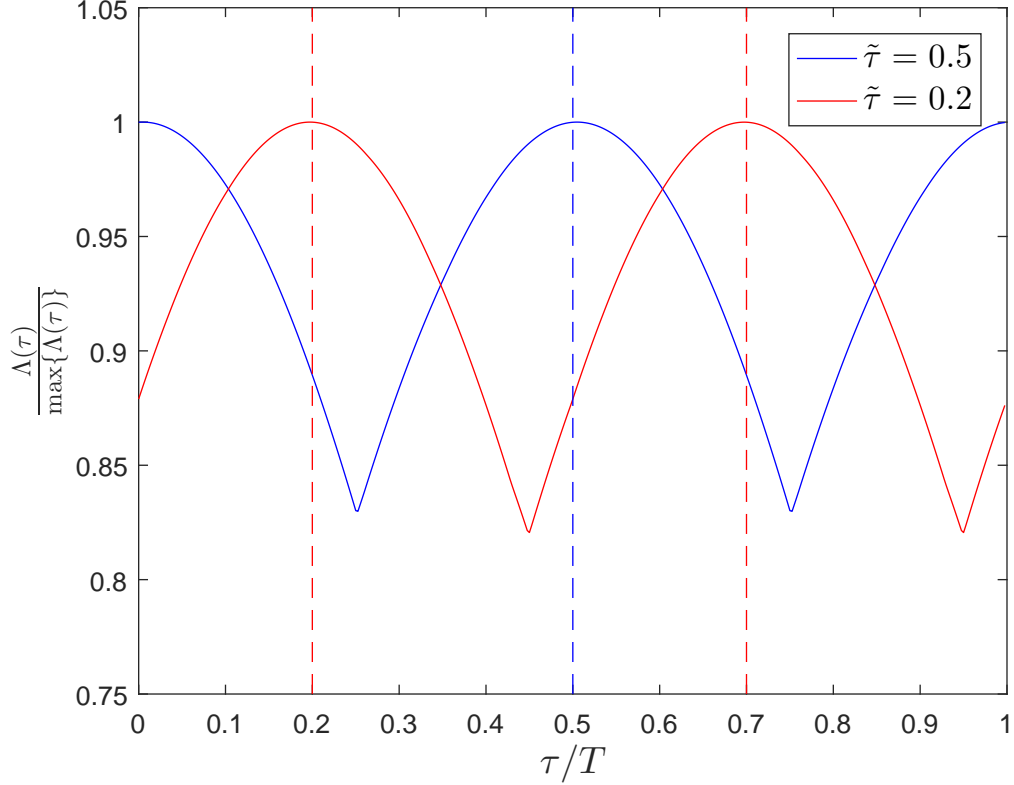


Figure 2.3: Typical shapes of the OQPSK CLF of the clock, $\Lambda(\tau)$.

$\tau_1 = \tau_1 + T/2$ and vice versa, as shown in Fig. 2.4. Changes refer to points that even a single bit of the sequence is different than that of the immediate previous point. Nevertheless, this doesn't lead to the same sequences between values of τ that are $T/2$ apart. In order to resolve this ambiguity of $\tilde{\tau}$ by multiples of $T/2$ our study was restricted to $[0, T/2)$ as practical reasons explained in Chapter 2.5 demand.

The first thing under our consideration is if the candidate set of the sequences at each step as well as the winning sequence remained constant for a number of adjacent points. The results made clear that the number of candidate set remains unchanged throughout a finite number of intervals and typically there are no winning sequences that reappear in $[0, T)$. This will prove to be very useful as a convergence criterion for the algorithm proposed in this study. However, the candidate set changes more frequently but this doesn't affect the detection. In addition, for an oversampling factor large enough, we have seen that only 1 bit changes from a winning sequence to the next one except from the extreme points of the shape. We have also experimented with different values of D_g to understand how Intersymbol interference (ISI) affects the detection.

Next, we focus in the angles of each bit of the sequence as defined in (2.45) and (2.46). As explained, in Chapter 2.3 the angle ϕ_i represents the angle for which the decision for the i -th bit changes. All of those angles are functions of τ in our equivalent problem of maximization and correspond to the arguments of the complex integrals as defined in (2.36) which leads us to test the assumption that when two of these angles intersect, exactly two members of the candidate set change. To illustrate, if $\phi_i < \phi_j$ for a given value of τ , say τ_1 , and for another value of τ , say $\tau_2 > \tau_1$, the only change in the angles sorted order is that now $\phi_i > \phi_j$ while the relative order of the rest of the angles didn't change then the two candidate sets should differ only at the sequence of the interval C_i at bit \hat{d}_i and the rest of the sequences are exactly the same. This was verified through simulations and an indicative shape of two angles that intersect at a

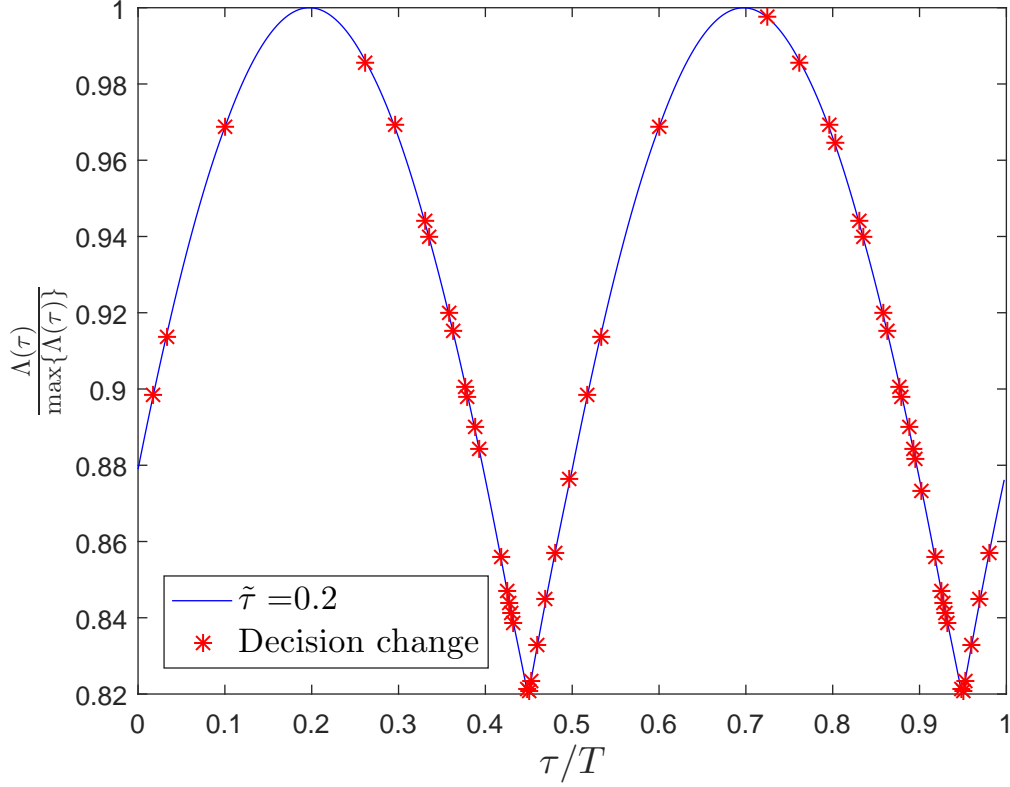


Figure 2.4: Points of candidate set changes.

point is shown in Fig. 2.5. This is exploited in the next section for the correlation of the angles.

Another statistical test we employed is to check whether for a lot of realizations the number the intervals created between the points that the pairs of angles intersect are less than or equal to $\binom{2(L_0+D_g)}{2}$ which would indicate that any pair of angles intersects at most one time during an interval of length $T/2$ and the solution of the equation would have unique solution. We remind at this point that $2(L_0 + D_g)$ is the total number of angles. The test didn't attest to this assumption.

2.5 Detection of sequence changes

Our goal at this point is to find the values of τ at which the estimated sequence changes. If we are able to do this efficiently we can visit only these points and obtain the optimal estimates for every $\tau \in [0, T)$. Actually, we have to correlate the angles of any pair of complex numbers defined in (2.36) in our effort to find all of the desired points. For any two complex numbers y_i, y_k and $i \neq k$ we have

$$\angle y_i = \angle y_k \Leftrightarrow \tan^{-1} \left(\frac{\Im \{y_i\}}{\Re \{y_i\}} \right) = \tan^{-1} \left(\frac{\Im \{y_k\}}{\Re \{y_k\}} \right) \quad (2.56)$$

$$\Leftrightarrow \frac{\Im \{y_i\}}{\Re \{y_i\}} = \frac{\Im \{y_k\}}{\Re \{y_k\}} \quad (2.57)$$

$$\Leftrightarrow \Im \{y_i\} \Re \{y_k\} = \Im \{y_k\} \Re \{y_i\} \quad (2.58)$$

$$\Leftrightarrow \Im \{y_i^* y_k\} = 0 \quad (2.59)$$

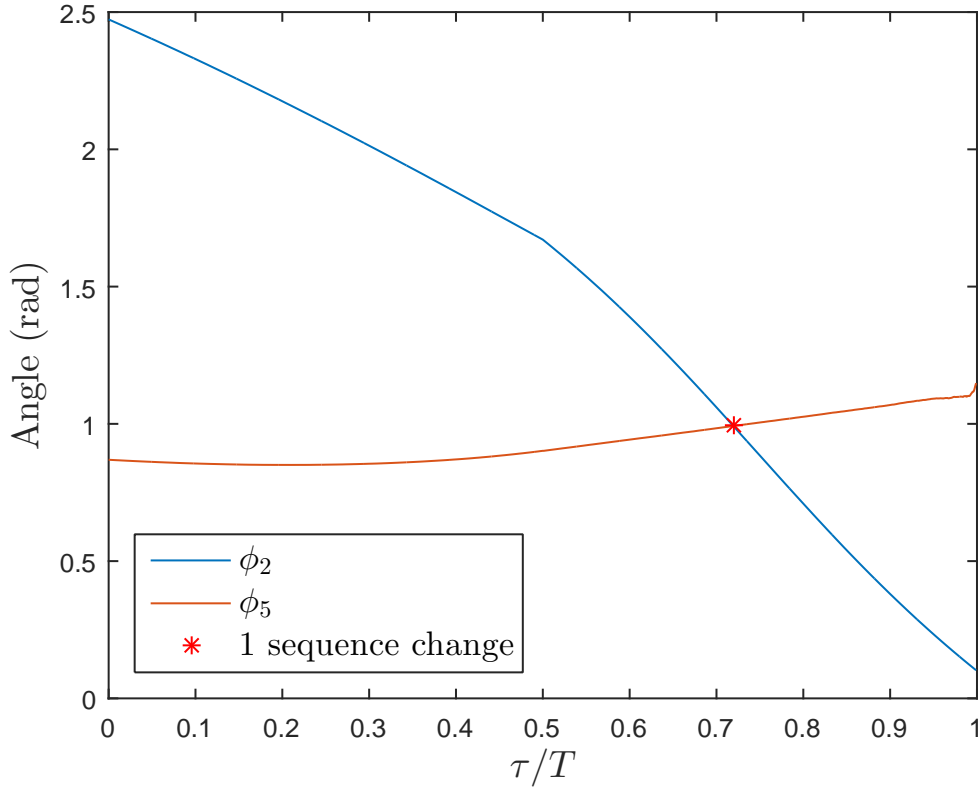


Figure 2.5: Typical shape of pair of decision change angles.

with (2.57) derived from the injectivity of $\tan^{-1}(\cdot)$ function on its domain. The set of complex numbers of (2.36) calculated for each value of τ is

$$y_i = \begin{cases} X_{-D_g+i/2}(\tau), & i = 0, 2, \dots, 2(L_0 + D_g) - 2 \\ -jX_{-D_g+(i-1)/2+1/2}(\tau), & i = 1, 3, \dots, 2(L_0 + D_g) - 1 \end{cases} \quad (2.60)$$

$$= \begin{cases} \int r(t)g(t - \tau - (-D_g + i/2)T)dt, & i \text{ even} \\ -j \int r(t)g(t - \tau - T/2 - (-D_g + (i-1)/2)T)dt, & i \text{ odd} \end{cases} \quad (2.61)$$

$$= \begin{cases} \int r(t)g(t - \tau - (-D_g + i/2)T)dt, & i \text{ even} \\ -j \int r(t)g(t - \tau - (-D_g + i/2)T)dt, & i \text{ odd} \end{cases} \quad (2.62)$$

for $i \in \{0, 1, \dots, 2(L_0 + D_g) - 1\}$. From (2.59) and (2.62) the correlation of the pairs of angles can be divided in four cases, as demonstrated below.

- Case 1: i, k even

$$(2.59) \stackrel{(2.62)}{\Leftrightarrow} \Im \left\{ \left(\int r^*(t)g(t - \tau - (-D_g + i/2)T)dt \right) \cdot \left(\int r(t)g(t - \tau - (-D_g + k/2)T)dt \right) \right\} = 0 \quad (2.63)$$

$$\Leftrightarrow \int \left(\int \left(R(F_1, F_2) G_{T_0}^*(F_1, F_2) \cdot e^{-j2\pi(F_1(\tau+(-D_g+i/2)T+F_2(\tau+(-D_g+k/2)T))} \right) dt_1 \right) dt_2 = 0 \quad (2.64)$$

For the analytical procedure, the reader can see A.7. The rest of the cases will be presented briefly since they follow the same derivation.

- Case 2: i even, k odd

$$(2.59) \stackrel{(2.62)}{\Leftrightarrow} \Im \left\{ \left(\int r^*(t)g(t - \tau - (-D_g + i/2)T)dt \right) \cdot \left(-j \int r(t)g(t - \tau - T/2 - (-D_g + (k-1)/2)T)dt \right) \right\} = 0 \quad (2.65)$$

$$\Leftrightarrow -\Re \left\{ \left(\int r^*(t)g(t - \tau - (-D_g + i/2)T)dt \right) \cdot \left(\int r(t)g(t - \tau - T/2 - (-D_g + (k-1)/2)T)dt \right) \right\} = 0 \quad (2.66)$$

$$\Leftrightarrow - \int \left(\int \left(R(F_1, F_2) G_{T_0}^*(F_1, F_2) \cdot e^{-j2\pi(F_1(\tau+(-D_g+i/2)T+F_2(\tau+T/2+(-D_g+(k-1)/2)T))} \right) dt_1 \right) dt_2 = 0 \quad (2.67)$$

- Case 3: i odd, k even

$$(2.59) \stackrel{(2.62)}{\Leftrightarrow} \Im \left\{ \left(-j \int r(t)g(t - \tau - T/2 - (-D_g + (i-1)/2)T)dt \right)^* \cdot \left(\int r(t)g(t - \tau - (-D_g + k/2)T)dt \right) \right\} = 0 \quad (2.68)$$

$$\Leftrightarrow \Re \left\{ \left(\int r(t)g(t - \tau - T/2 - (-D_g + (i-1)/2)T)dt \right) \cdot \left(\int r(t)g(t - \tau - (-D_g + k/2)T)dt \right) \right\} = 0 \quad (2.69)$$

$$\Leftrightarrow - \int \left(\int \left(R(F_1, F_2) G_{T_0}^*(F_1, F_2) \cdot e^{-j2\pi(F_1(\tau+T/2(-D_g+(i-1)/2)T+F_2(\tau+(-D_g+k/2)T))} \right) dt_1 \right) dt_2 = 0 \quad (2.70)$$

- Case 4: i, k odd

$$(2.59) \stackrel{(2.62)}{\Leftrightarrow} \Im \left\{ \left(-j \int r(t)g(t - \tau - T/2 - (-D_g + (i-1)/2)T)dt \right)^* \cdot \left(-j \int r(t)g(t - \tau - T/2 - (-D_g + (k-1)/2)T)dt \right) \right\} = 0 \quad (2.71)$$

$$\Leftrightarrow - \int \left(\int \left(R(F_1, F_2) G_{T_0}^*(F_1, F_2) \cdot e^{-j2\pi(F_1(\tau+T/2(-D_g+(i-1)/2)T+F_2(\tau+T/2+(-D_g+(k-1)/2)T))} \right) dt_1 \right) dt_2 = 0 \quad (2.72)$$

In cases 1 and 4

$$r(t_1, t_2) = \Im \{ r^*(t_1)r(t_2) \} \quad (2.73)$$

while in cases 2 and 3

$$r(t_1, t_2) = \Re \{ r^*(t_1)r(t_2) \} \quad (2.74)$$

As stated earlier our study is focused on $\tau \in [0, T/2]$. The reason for our choice of this interval over any other interval of length $T/2$ is that the correlation between any angle and the angle of y_i with the greatest index, i.e. $i = 2(L_0 + D_g) - 1$, is not possible because the latter goes to zero as proven below

$$y_i \Big|_{i=2(L_0+D_g)-1} = -jX_{-D_g+L_0+D_g-1+1/2}(\tau) \quad (2.75)$$

$$= -jX_{L_0-1+1/2}(\tau) \quad (2.76)$$

$$= \int_0^{T_0} r(t)g(t - \tau - T/2 - (L_0 - 1)T)dt \quad (2.77)$$

$$= \int_0^{L_0T} r(t)g(t - L_0T - \tau + T/2)dt \quad (2.78)$$

This expression is zero for $\tau \geq T/2$. We can elucidate in the four cases even further which leads to convolution domain.

- Case 1: i, k even

$$(A.43) \Leftrightarrow \int \int H(F_1, F_2) e^{-j2\pi(F_1(\tau+(-D_g+i/2)T)+F_2(\tau+(-D_g+k/2)T))} dF_1 dF_2 = 0 \quad (2.79)$$

$$\Leftrightarrow h(-\tau - (-D_g + i/2)T, -\tau - (-D_g + k/2)T) = 0 \quad (2.80)$$

$$\Leftrightarrow \left[r(t_1, t_2) * * g^*(t_1, t_2) \right]_{t_1=-\tau-(-D_g+i/2)T, t_2=-\tau-(-D_g+k/2)T} = 0 \quad (2.81)$$

$$\Leftrightarrow \left[r(t_1, t_2) * * g(t_1, t_2) \right]_{t_1=-\tau-(-D_g+i/2)T, t_2=-\tau-(-D_g+k/2)T} = 0 \quad (2.82)$$

- Case 2: i even, k odd

$$(2.67) \Leftrightarrow - \int \int H(F_1, F_2) e^{-j2\pi(F_1(\tau+(-D_g+i/2)T)+F_2(\tau+(-D_g+T/2+(k-1)/2)T))} dF_1 dF_2 = 0 \quad (2.83)$$

$$\Leftrightarrow \left[r(t_1, t_2) * * g(t_1, t_2) \right]_{t_1=-\tau-(-D_g+i/2)T, t_2=-\tau-T/2-(-D_g+(k-1)/2)T} = 0 \quad (2.84)$$

- Case 3: i odd, k even

$$(2.70) \Leftrightarrow \int \int H(F_1, F_2) e^{-j2\pi(F_1(\tau+T/2+(-D_g+(i-1)/2)T)+F_2(\tau+(-D_g+k/2)T))} dF_1 dF_2 = 0 \quad (2.85)$$

$$\Leftrightarrow \left[r(t_1, t_2) * * g(t_1, t_2) \right]_{t_1=-\tau-T/2-(-D_g+(i-1)/2)T, t_2=-\tau-(-D_g+k/2)T} = 0 \quad (2.86)$$

- Case 4: i, k odd

$$(2.72) \Leftrightarrow \int \int H(F_1, F_2) e^{-j2\pi(F_1(\tau+T/2+(-D_g+(i-1)/2)T)+F_2(\tau+T/2+(-D_g+(k-1)/2)T))} dF_1 dF_2 = 0 \quad (2.87)$$

$$\Leftrightarrow \left[r(t_1, t_2) * * g(t_1, t_2) \right]_{t_1=-\tau-T/2-(-D_g+(i-1)/2)T, t_2=-\tau-T/2-(-D_g+(k-1)/2)T} = 0 \quad (2.88)$$

where

$$h(t_1, t_2) = r(t_1, t_2) ** g_{T_0}^*(t_1, t_2) \quad (2.89)$$

$$H(F_1, F_2) = \mathcal{F} \{h(t_1, t_2)\} \quad (2.90)$$

and (2.82) is because $g(t)$ is a real-valued function. From (2.82), (2.84), (2.86) and (2.88) it is evident that we do not need to calculate the whole two-dimension grid of the convolution but we should limit our search to a diagonal of the grid thereby maximizing a one-dimensional function. Despite that, we still have to go through all of the values of τ in order to find the points at which the estimation changes.

2.6 Noncoherent detection algorithm and results

Using the properties noted in Chapter 2.4, we can resort to a gradient descent algorithm and we should start by taking the first-order derivative of the likelihood of (2.37) with respect to τ

$$\begin{aligned} \Lambda(\tau) = & \sum_{i=-D_g}^{L_0-1} \left\{ \sum_{k=-D_g}^{L_0-1} \left\{ \hat{a}_i(\tau) X_i(\tau) \hat{a}_k(\tau) X_k^*(\tau) \right\} \right\} \\ & + j \sum_{i=-D_g}^{L_0-1} \left\{ \sum_{k=-D_g}^{L_0-1} \left\{ \hat{a}_i(\tau) X_i(\tau) \hat{b}_k(\tau) X_{k+1/2}^*(\tau) \right\} \right\} \\ & - j \sum_{i=-D_g}^{L_0-1} \left\{ \sum_{k=-D_g}^{L_0-1} \left\{ \hat{b}_i(\tau) X_{i+1/2}(\tau) \hat{a}_k(\tau) X_k^*(\tau) \right\} \right\} \\ & + \sum_{i=-D_g}^{L_0-1} \left\{ \sum_{k=-D_g}^{L_0-1} \left\{ \hat{b}_i(\tau) X_{i+1/2}(\tau) \hat{b}_k(\tau) X_{k+1/2}^*(\tau) \right\} \right\} \end{aligned} \quad (2.91)$$

after some simple calculations given in B.7. The derivative of this quantity is

$$\begin{aligned} \frac{\partial \Lambda(\tau)}{\partial \tau} = & \sum_{i=-D_g}^{L_0-1} \left\{ \sum_{k=-D_g}^{L_0-1} \left\{ \hat{a}_i(\tau) \hat{a}_k(\tau) \left[\frac{\partial X_i(\tau)}{\partial \tau} X_k^*(\tau) + X_i(\tau) \frac{\partial X_k^*(\tau)}{\partial \tau} \right] \right\} \right\} \\ & + j \sum_{i=-D_g}^{L_0-1} \left\{ \sum_{k=-D_g}^{L_0-1} \left\{ \hat{a}_i(\tau) \hat{b}_k(\tau) \left[\frac{\partial X_i(\tau)}{\partial \tau} X_{k+1/2}^*(\tau) + X_i(\tau) \frac{\partial X_{k+1/2}^*(\tau)}{\partial \tau} \right] \right\} \right\} \\ & - j \sum_{i=-D_g}^{L_0-1} \left\{ \sum_{k=-D_g}^{L_0-1} \left\{ \hat{b}_i(\tau) \hat{a}_k(\tau) \left[\frac{\partial X_{i+1/2}(\tau)}{\partial \tau} X_k^*(\tau) + X_{i+1/2}(\tau) \frac{\partial X_k^*(\tau)}{\partial \tau} \right] \right\} \right\} \\ & + \sum_{i=-D_g}^{L_0-1} \left\{ \sum_{k=-D_g}^{L_0-1} \left\{ \hat{b}_i(\tau) \hat{b}_k(\tau) \left[\frac{\partial X_{i+1/2}(\tau)}{\partial \tau} X_{k+1/2}^*(\tau) + X_{i+1/2}(\tau) \frac{\partial X_{k+1/2}^*(\tau)}{\partial \tau} \right] \right\} \right\} \end{aligned} \quad (2.92)$$

where the first-order derivatives are calculated based on the Leibnitz's rule and the derivative of the SRRC wave of (2.3) which is

$$\begin{aligned} \frac{\partial g(t)}{\partial t} = & \frac{4\alpha}{\pi\sqrt{T}} \left(\frac{-\sin((1+\alpha)\pi t/T)(1+\alpha)\pi/T(1-(4\alpha T/t)^2) + 32\alpha^2 t/T^2 \cos((1+\alpha)\pi t/T)}{(1-(4\alpha t/T)^2)^2} \right. \\ & \left. + \frac{\frac{\cos((1-\alpha)\pi t/T)(1-\alpha)\pi/T 4\alpha t/T - 4\alpha/T \sin((1-\alpha)\pi t/T)}{(4\alpha t/T)^2} (1-(4\alpha t/T)^2) + 32\alpha^2 t/T^2 \frac{\sin((1-\alpha)\pi t/T)}{4\alpha t/T}}{(1-(4\alpha t/T)^2)^2} \right) \end{aligned} \quad (2.93)$$

The algorithm we propose for the detection is given in Fig. 2.6. We start by randomly selecting an initial value of τ and at each step the derivative of the CLF at the current point is obtained. If the derivative is positive, the direction we move is towards larger values of τ at each iteration by a predefined step, represented by τ_step , and towards the opposite direction for negative values of the derivative. If the next point lies outside of the boundaries, already discussed to be $\tau \in [0, T/2)$, we can bring it to the utilized range. If at some point the derivative has changed from a negative sign to a positive one, then the likelihood is maximized at a value of τ residing between those two points. After this iteration, a sufficient terminating criterion would be a sign change of the derivative combined with the demand that the estimated sequence between consecutive steps to remain unchanged. Indeed, since no sequence reappears in disjoint intervals, as noted previously, that would be exactly the ML sequence that the procedure returns. The complexity of this algorithm is dominated by the calculation of the integrals of the derivative, for which we didn't find an efficient way to compute faster, while the cost of the detection at each point is $\mathcal{O}((N+1)\log_2(N+1)) \approx \mathcal{O}(N\log N)$, as stated earlier. N represents the sequence length.

In Fig. 2.7 we have illustrated the trajectory for one realization of the gradient descent method and for fixed values of the channel parameters \tilde{h} , $\tilde{\theta}$ and $\tilde{\tau}$. The solid red line represents the point of maximum while the corresponding trajectory is shown green on the figure and the last point's estimate didn't change compared to the previous one whereas the sign of the derivative was inverted denoting the termination of the procedure.

Algorithm 2 Noncoherent OQPSK Sequence Detection

Input: $\hat{\mathbf{a}}(\tau), \hat{\mathbf{b}}(\tau)$

```
1:  $\tau_*$  := a random real in  $[0, T/2)$ 
2:  $\tau_c := \tau_*$ 
3:  $i := 0$ 
4: while 1 do
5:    $D = \frac{\vartheta\Lambda(\tau_c)}{\vartheta\tau}$ 
6:   if  $i \geq 1$  then
7:     if  $\text{sign}(D) = -\text{sign}(D_p)$  then
8:        $\tau\_step := \lceil \frac{\tau\_step}{2} \rceil$ 
9:       if  $\hat{\mathbf{a}}(\tau_c) = \hat{\mathbf{a}}_p$  and  $\hat{\mathbf{b}}(\tau_c) = \hat{\mathbf{b}}_p$  then
10:         $\hat{\mathbf{a}}\_ML := \hat{\mathbf{a}}_p$ 
11:         $\hat{\mathbf{b}}\_ML := \hat{\mathbf{b}}_p$ 
12:        break
13:      end if
14:    end if
15:  end if
16:   $\hat{\mathbf{a}}_p := \hat{\mathbf{a}}(\tau)$ 
17:   $\hat{\mathbf{b}}_p := \hat{\mathbf{b}}(\tau)$ 
18:  if  $D > 0$  then
19:     $\tau_c := \tau_c + \tau\_step$ 
20:  else if  $D < 0$  then
21:     $\tau_c := \tau_c - \tau\_step$ 
22:  else
23:    break
24:  end if
25:  if  $\tau_c \geq \frac{T}{2}$  then
26:     $\tau_c := \text{mod}(\tau_c, \frac{T}{2})$ 
27:  else if  $\tau_c < 0$  then
28:     $\tau_c := \tau_c + \frac{T}{2}$ 
29:  end if
30:   $D_p := D$ 
31:   $i := i + 1$ 
32: end while
```

Figure 2.6: Proposed noncoherent OQPSK sequence detection algorithm.

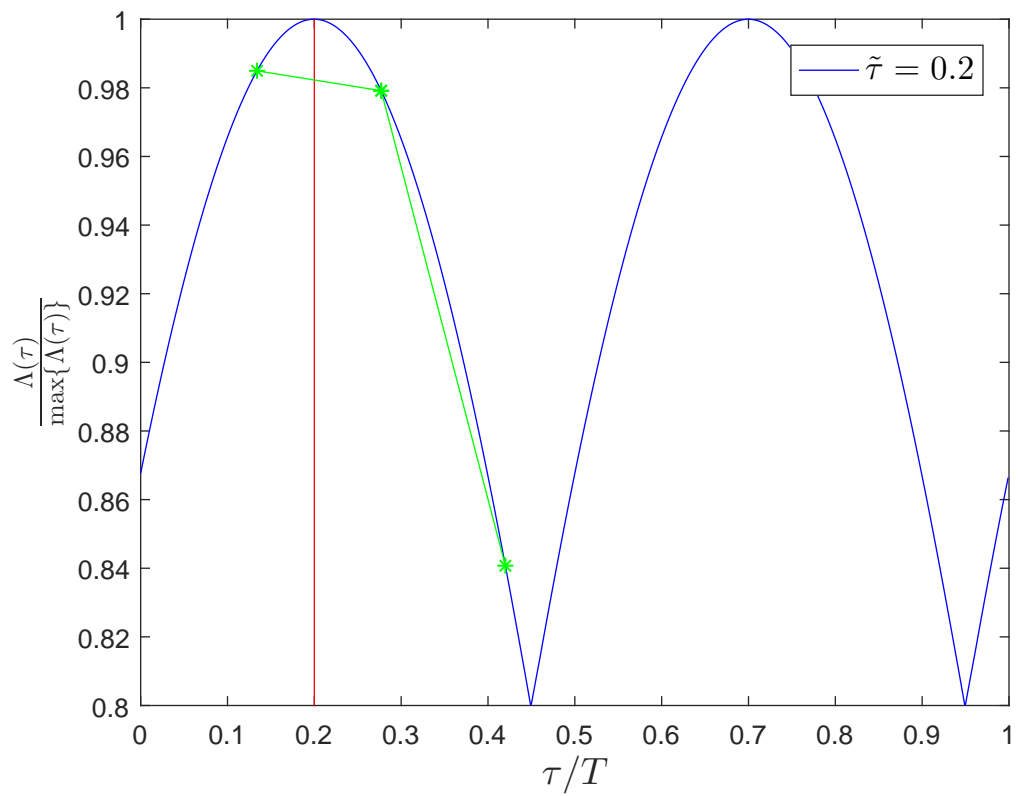


Figure 2.7: Gradient descent trajectory of noncoherent detection in OQPSK.

Detection in FSK

3.1 Signal model

The BFSK channel utilizes two frequencies, namely F_{-1} and F_1 , each of which is matched to a specific symbol. The symbols are binary and $x_i \in \{\pm 1\}$ without loss of generality. The transmitted FSK waveform is

$$s(t) = \sum_i g_{x_i}(t - iT)u_T(t - iT) \quad (3.1)$$

with

$$g_{x_i}(t) = \sqrt{\frac{P}{T}} e^{j2\pi F_{x_i} t} \quad (3.2)$$

where P is the signal strength and T is the nominal duration of each symbol while $u_T(t - x)$ stands for a square pulse of duration T starting at $t = x$ like

$$u_T(t - x) = \begin{cases} 1, & x \leq t < x + T \\ 0, & \text{otherwise} \end{cases} \quad (3.3)$$

The orthogonality condition that non-coherent BFSK should respect is

$$|F_{-1} - F_1| = kT \quad (3.4)$$

for $k \in \mathbb{Z}$ and $k \geq 1$. The channel is assumed flat-fading and thus the received signal is

$$r(t) = \tilde{h}s(t - \tilde{\tau}) + n(t) \quad (3.5)$$

Here $\tilde{h} \in \mathbb{C}$ is generated randomly, the attenuation is set to its absolute value and the channel phase change is set to its argument and $n(t)$ is a zero-mean complex Gaussian process with unary variance.

3.2 The likelihood function

The same derivation as the one used in Chapter 2.2 leads to the following CLF

$$\Lambda(\mathbf{x}, \tau) = \left| \int_0^{T_0} r(t) s^*(t - \tau) dt \right|^2 \quad (3.6)$$

$$\begin{aligned}
&= \left| \sum_{i=-1}^{L_0-1} \left\{ x_i \left[\int_0^{T_0} \frac{r(t)}{2} \sqrt{\frac{P}{T}} e^{-j2\pi F_1(t-\tau-iT)} u_T(t-\tau-iT) dt - \dots \right. \right. \right. \\
&\quad \left. \left. \left. \dots - \int_0^{T_0} \frac{r(t)}{2} \sqrt{\frac{P}{T}} e^{-j2\pi F_{-1}(t-\tau-iT)} u_T(t-\tau-iT) dt \right] \right\} + \dots \right. \\
&\quad \left. \dots + \sum_{i=-1}^{L_0-1} \left\{ \int_0^{T_0} \frac{r(t)}{2} \sqrt{\frac{P}{T}} e^{-j2\pi F_{-1}(t-\tau-iT)} u_T(t-\tau-iT) dt + \dots \right. \right. \\
&\quad \left. \left. \left. \dots + \int_0^{T_0} \frac{r(t)}{2} \sqrt{\frac{P}{T}} e^{-j2\pi F_1(t-\tau-iT)} u_T(t-\tau-iT) dt \right\} \right|^2 \quad (3.7)
\end{aligned}$$

The proof for this likelihood is in B.1.

3.3 Likelihood maximization

Calculations similar to those of Chapter 2.3 show that the problem of maximizing the quantity in (3.7) is actually to find the binary sequence $\mathbf{d} \in \{\pm 1\}^{N+2,1}$ which for a given complex vector $\mathbf{y}' \in \mathbb{C}^{N+1,1}$ and $z \in \mathbb{C}$ maximizes the quantity $|\mathbf{d}^T [\mathbf{y}' \quad z]|$ since the initial problem is

$$\max_{\mathbf{d}' \in \{\pm 1\}^{N+1}} |\mathbf{d}'^T \mathbf{y}' + z| = \max_{\mathbf{d}' \in \{\pm 1\}^{N+1}, d_{N+1} \in \{\pm 1\}} |d_0 y_0 + d_1 y_1 + \dots + d_N y_N + d_{N+1} z| \quad (3.8)$$

$$= \max_{\mathbf{d} \in \{\pm 1\}^{N+2}} |\mathbf{d}^T \mathbf{y}| \quad (3.9)$$

where

$$\mathbf{d} = \begin{bmatrix} \mathbf{d}' \\ d_{N+1} \end{bmatrix} \quad (3.10)$$

and

$$\mathbf{y} = \begin{bmatrix} \mathbf{y}' \\ z \end{bmatrix} \quad (3.11)$$

and for (3.7) we set

$$y_i = \int_0^{T_0} \frac{r(t)}{2} \sqrt{\frac{P}{T}} e^{-j2\pi F_1(t-\tau-iT)} u_T(t-\tau-iT) dt - \int_0^{T_0} \frac{r(t)}{2} \sqrt{\frac{P}{T}} e^{-j2\pi F_{-1}(t-\tau-iT)} u_T(t-\tau-iT) dt \quad (3.12)$$

Also

$$z = \sum_{i=-1}^{L_0-1} \left\{ \int_0^{T_0} \frac{r(t)}{2} \sqrt{\frac{P}{T}} e^{-j2\pi F_{-1}(t-\tau-iT)} u_T(t-\tau-iT) dt + \int_0^{T_0} \frac{r(t)}{2} \sqrt{\frac{P}{T}} e^{-j2\pi F_1(t-\tau-iT)} u_T(t-\tau-iT) dt \right\} \quad (3.13)$$

having $\mathbf{d} = [\mathbf{x} \quad 1]^T$. In other words, the only extra requirement we need to impose is that the last bit is +1. This is straightforward for the implementation by keeping the sequence of length $N + 2 = L_0 + 2$ that the algorithm returns if it ends with a +1, otherwise inverting it. Both sequences will give the same

metric, as explained earlier. Thus, if we were merely interested in synchronization this change wouldn't matter. As a result, the complex numbers that the algorithm takes as input in (A.22) are (as proved in B.2)

$$y_{i+1} = \begin{cases} \frac{1}{2} \sqrt{\frac{P}{T}} \int_0^{T_0} r(t) \left[e^{-j2\pi F_1(t-\tau-iT)} - e^{-j2\pi F_1(t-\tau-iT)} \right] u_T(t-\tau-iT) dt, & i = -1, 0, \dots, L_0 - 1 \\ \sum_{a=-1}^{L_0-1} \left\{ \frac{1}{2} \sqrt{\frac{P}{T}} \int_0^{T_0} r(t) \left[e^{-j2\pi F_1(t-\tau-aT)} + e^{-j2\pi F_1(t-\tau-aT)} \right] u_T(t-\tau-aT) dt \right\}, & i = L_0 \end{cases} \quad (3.14)$$

3.4 Detection of sequence changes

At this point we have made the same observations as those explained in Chapters 2.4 and 2.5 and we can now correlate the angles of the complex numbers in (3.14) resorting to two cases. For $y_{i+1}, y_{k+1} \in \mathbb{C}$ and $i \neq k$ we have

$$\angle y_{i+1} = \angle y_{k+1} \Leftrightarrow \Im \{ y_{i+1}^* y_{k+1} \} = 0 \quad (3.15)$$

The derivation follows along the same principles with that of Chapter 2.5 and is presented here briefly.

- Case 1: $i, k \in \{-1, 0, \dots, L_0 - 1\}$

$$(3.15) \stackrel{(3.14)}{\Leftrightarrow} \Im \left\{ \left[\frac{1}{2} \sqrt{\frac{P}{T}} \int_0^{T_0} r^*(t) \left[e^{j2\pi F_1(t-\tau-iT)} - e^{j2\pi F_1(t-\tau-iT)} \right] u_T(t-\tau-iT) dt \right] \left[\frac{1}{2} \sqrt{\frac{P}{T}} \int_0^{T_0} r(t) \left[e^{-j2\pi F_1(t-\tau-kT)} - e^{-j2\pi F_1(t-\tau-kT)} \right] u_T(t-\tau-kT) dt \right] \right\} = 0 \quad (3.16)$$

$$\Leftrightarrow \int_0^{T_0} \left(\int_0^{T_0} \left(R(F_a, F_b) G^*(F_a, F_b) e^{-j4\pi(F_a(\tau+iT)+F_b(\tau+kT))} \right) dF_a \right) dF_b = 0 \quad (3.17)$$

as shown in B.3.

- Case 2: $i \in \{-1, 0, \dots, L_0 - 1\}$ and $k = L_0$

$$(3.15) \stackrel{(3.14)}{\Leftrightarrow} \Im \left\{ \left[\frac{1}{2} \sqrt{\frac{P}{T}} \int_0^{T_0} r^*(t) \left[e^{j2\pi F_1(t-\tau-iT)} - e^{j2\pi F_1(t-\tau-iT)} \right] u_T(t-\tau-iT) dt \right] \left[\sum_{a=-1}^{L_0-1} \left\{ \frac{1}{2} \sqrt{\frac{P}{T}} \int_0^{T_0} r(t) \left[e^{-j2\pi F_1(t-\tau-aT)} + e^{-j2\pi F_1(t-\tau-aT)} \right] u_T(t-\tau-aT) dt \right\} \right] \right\} = 0 \quad (3.18)$$

$$\Leftrightarrow \sum_{m=-1}^{L_0-1} \left\{ \int_0^{T_0} \left(\int_0^{T_0} \left(R(F_a, F_b) G^*(F_a, F_b) e^{-j4\pi(F_a(\tau+iT)+F_b(\tau+mT))} \right) dF_a \right) dF_b \right\} = 0 \quad (3.19)$$

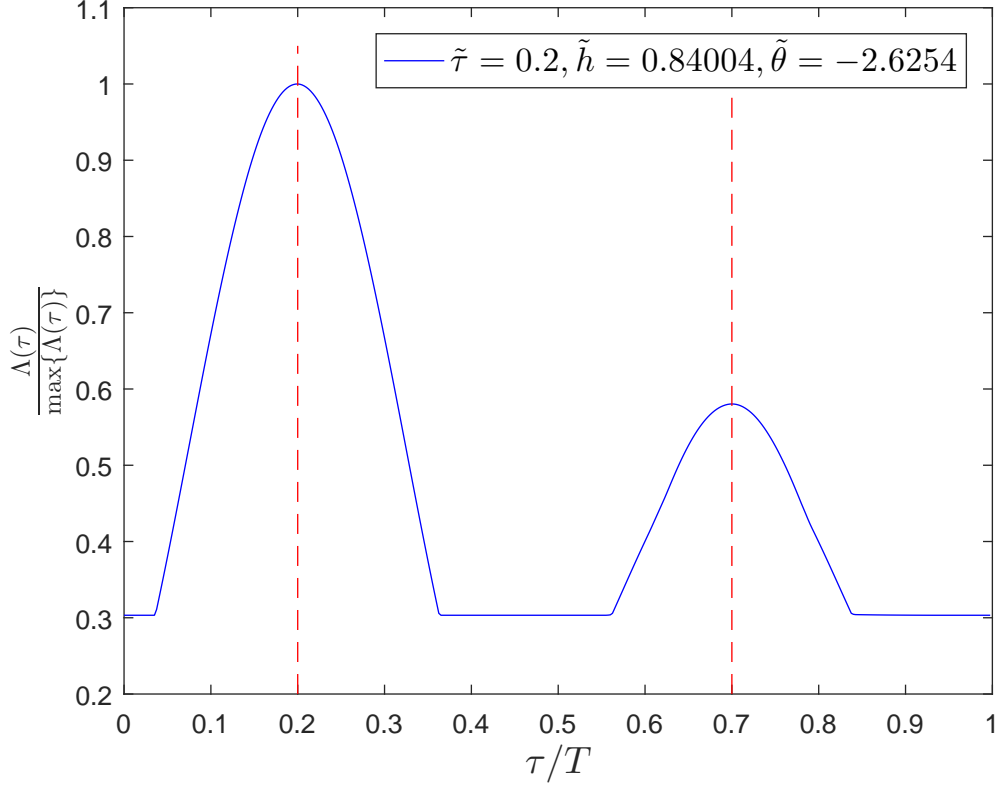


Figure 3.1: Shape of the BFSK CLF of the clock $\Lambda(\tau)$ for $\lambda = 2$ with two local maxima.

as shown in B.4 where

$$r(t_1, t_2) = \Im \left\{ r^*(t_1) \left[e^{j2\pi F_1 t_1} - e^{j2\pi F_{-1} t_1} \right] r(t_2) \left[e^{-j2\pi F_1 t_2} - e^{-j2\pi F_{-1} t_2} \right] \right\} \quad (3.20)$$

$$R(F_a, F_b) = \mathcal{F} \{ r(t_1, t_2) \} \quad (3.21)$$

$$G^*(F_a, F_b) = \mathcal{F} \{ (u_T(t_1) u_T(t_2))^* \} = \mathcal{F} \{ u_T(t_1) u_T(t_2) \} \quad (3.22)$$

3.5 Likelihood properties, noncoherent detection algorithm and results

For the simulations the frequencies used for the binary symbols were $1/T$ and $2/T$. This is because in our tests, we have seen that the number of maximums of the BFSK's likelihood shape is the same as the ratio of the smallest of the absolute values of the frequencies to the symbol frequency $1/T$ i.e.

$$\lambda = \frac{\min \{ |F_{-1}|, |F_1| \}}{1/T} \quad (3.23)$$

and that the local maxima appear at equidistant points and more precisely at the points

$$\tau_i = \tilde{\tau} + (i-1) \frac{T}{\lambda} \pmod{T}, \quad i \in \{1, \dots, \lambda\} \quad (3.24)$$

This is shown in Fig. 3.1 for $\tau = 0.5$. Consequently, we wanted to focus in those cases with only one maximum ($\lambda = 1$) which are for $(F_{-1}, F_1) = (1/T, 2/T)$ and $(F_{-1}, F_1) = (-1/T, -2/T)$ sticking to the former without loss of generality. Another reason for that is that in contrast to other options

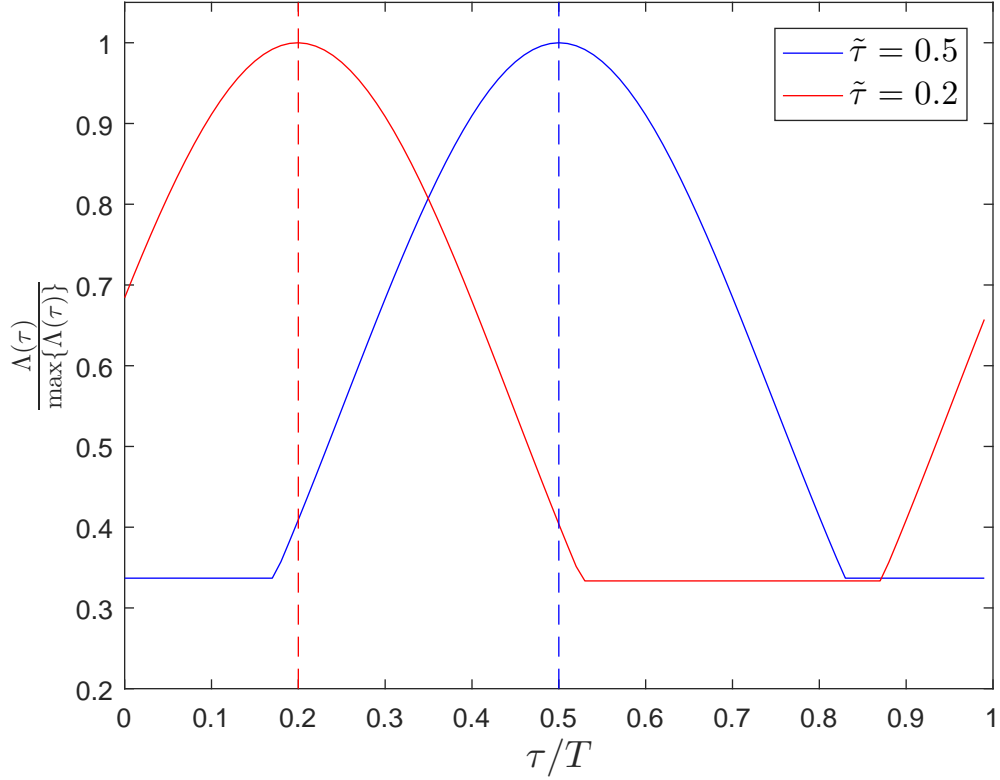


Figure 3.2: Typical shapes of the BFSK CLF of the clock $\Lambda(\tau)$.

there are no sequences that reappear in disjoint intervals of τ . The SNR is set to 30dB and the symbols transmitted are $L_0 = 100$ in total. Typical shapes of the CLF for two values of τ are in Fig. 3.2. We can see that they are maximized at the actual delays, as expected. Also their value is constant across some intervals. In this case, the winning sequences happen to be either $\mathbf{d}^T = [\mathbf{x} \ 1] = [-\mathbf{1}^{L_0+1} \ 1]$ or $\mathbf{d}^T = [\mathbf{x} \ 1] = [\mathbf{1}^{L_0+1} \ 1]$ and at Chapter B.5 a proof of this property is attached. The existence of only one maximum leads us to employ a gradient descent method in our algorithm for detection as we did in OQPSK. The first step is to calculate the first-order derivative of the CLF with respect to τ . The problem that arises here is that the flat regions of the shape would render gradient descent susceptible to approximation issues. To overcome this obstacle, we calculated and plotted the following function, say $\Lambda_2(\tau)$ by eliminating the first summation from $\Lambda(\mathbf{x}, \tau)$ which is independent of the sequence estimates. Through simulations, we have verified that $\Lambda(\mathbf{x}, \tau)$ and $\Lambda_2(\tau)$ are maximized at the same values of τ (without proof).

$$\Lambda_2(\tau) = \left| \sum_{i=-1}^{L_0-1} \left\{ \int_0^{T_0} \frac{r(t)}{2} \sqrt{\frac{P}{T}} e^{-j2\pi F_{-1}(t-\tau-iT)} u_T(t-\tau-iT) dt + \dots \right. \right. \\ \left. \left. \dots + \int_0^{T_0} \frac{r(t)}{2} \sqrt{\frac{P}{T}} e^{-j2\pi F_1(t-\tau-iT)} u_T(t-\tau-iT) dt \right\} \right|^2 \quad (3.25)$$

$$= \frac{1}{4} \frac{P}{T} \sum_{i=-1}^{L_0-1} \left\{ \sum_{k=-1}^{L_0-1} \left\{ I(\tau; F_{-1}, i) I_c(\tau; F_{-1}, k) + I(\tau; F_{-1}, i) I_c(\tau; F_1, k) + \dots \right. \right. \\ \left. \left. \dots + I(\tau; F_1, i) I_c(\tau; F_{-1}, k) + I(\tau; F_1, i) I_c(\tau; F_1, k) \right\} \right\} \quad (3.26)$$

and a proof can be found at B.6 where we defined the integrals

$$I(\tau; F, i) = \int_0^{T_0} r(t) e^{-j2\pi F(t-\tau-iT)} u_T(t-\tau-iT) dt \quad (3.27)$$

and

$$I_c(\tau; F, i) = \int_0^{T_0} r^*(t) e^{j2\pi F(t-\tau-iT)} u_T(t-\tau-iT) dt \quad (3.28)$$

Then (for a proof see B.7)

$$\frac{\partial I(\tau; F, i)}{\partial \tau} = \int_0^{T_0} r(t) j2\pi F e^{-j2\pi F(t-\tau-iT)} u_T(t-\tau-iT) dt + r_\delta(\tau+iT) + r_\delta(\tau+iT+T) e^{-j2\pi FT} \quad (3.29)$$

for

$$r_\delta(t) = \begin{cases} r(t), & t \in [0, T_0] \\ 0, & \text{otherwise} \end{cases} \quad (3.30)$$

Similarly

$$\frac{\partial I_c(\tau; F, i)}{\partial \tau} = - \int_0^{T_0} r^*(t) j2\pi F e^{j2\pi F(t-\tau-iT)} u_T(t-\tau-iT) dt + r_\delta^*(\tau+iT) + r_\delta^*(\tau+iT+T) e^{j2\pi FT} \quad (3.31)$$

The first-order derivative of $\Lambda_2(\tau)$ with respect to τ is

$$\frac{\partial \Lambda_2(\tau)}{\partial \tau} = \frac{1}{4} \frac{P}{T} \sum_{i=-1}^{L_0-1} \left\{ \sum_{k=-1}^{L_0-1} \left\{ \frac{\partial I(\tau; F_{-1}, i)}{\partial \tau} I_c(\tau; F_{-1}, k) + I(\tau; F_{-1}, i) \frac{\partial I_c(\tau; F_{-1}, k)}{\partial \tau} + \dots \right. \right. \quad (3.32)$$

$$\dots + \frac{\partial I(\tau; F_1, k)}{\partial \tau} I_c(\tau; F_{-1}, k) + I(\tau; F_{-1}, i) \frac{\partial I_c(\tau; F_1, k)}{\partial \tau} + \dots \quad (3.33)$$

$$\dots + \frac{\partial I(\tau; F_1, i)}{\partial \tau} I_c(\tau; F_{-1}, k) + I(\tau; F_1, i) \frac{\partial I_c(\tau; F_{-1}, k)}{\partial \tau} + \dots \quad (3.34)$$

$$\dots + \frac{\partial I(\tau; F_1, i)}{\partial \tau} I_c(\tau; F_1, k) + I(\tau; F_1, i) \frac{\partial I_c(\tau; F_1, k)}{\partial \tau} \left. \right\} \quad (3.35)$$

and all of the required partial derivatives will be calculated according to (3.29) and (3.31). The proposed algorithm is essentially the same as the one implemented for the BFSK in Chapter 2.6 and is therefore omitted. The complexity of this algorithm is dominated by the calculation of the integrals of the derivative, for which we didn't find an efficient way to compute faster, while the cost of the detection at each point is $\mathcal{O}((N+1) \log_2(N+1)) \approx \mathcal{O}(N \log N)$, as in the case of OQPSK. N represents the sequence length.

At the Fig.3.4 we can see the Bit-error-rate (BER) (for various values of L_0) versus a range of possible SNR values. The performance is improved for larger values of the observation interval and as SNR increases.

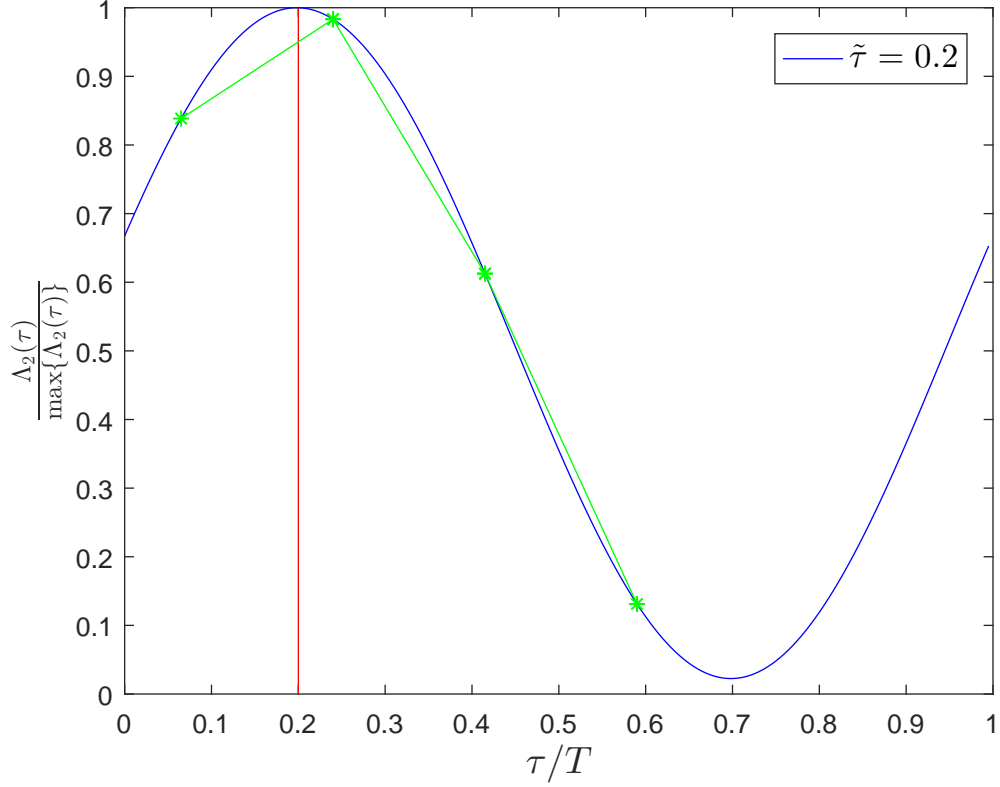


Figure 3.3: Gradient descent trajectory of noncoherent detection in BFSK.

The BER of the corresponding coherent channel utilizing the ML detector and with known parameters $\tilde{\tau}$, \tilde{h} and $\tilde{\theta}$ has also been included in the figure as a reference and is explained in Chapter 3.6. We observe that, as the sequence length increases, the noncoherent detector approaches the coherent one in terms of BER.

The trajectory that the gradient descent method traverses (for one realization) can be seen in Fig. 3.3 for a single realization and for fixed values of the channel parameters \tilde{h} , $\tilde{\theta}$ and $\tilde{\tau}$, similarly to the case of OQPSK modulation.

3.6 Coherent detection

The optimal receiver correlates $r(t)$ with both signalling waveforms to produce samples

$$r_m = \frac{1}{\sqrt{P}} \int_0^T r(t)g_{x_i}^*(t)dt, \quad m = -1, 1. \quad (3.36)$$

$$= \frac{1}{\sqrt{P}} \int_0^T (\tilde{h}g_{x_i}(t) + n(t))g_{x_i}^*(t)dt \quad (3.37)$$

$$= \frac{\tilde{h}}{\sqrt{P}} \int_0^T |g_{x_i}(t)|^2 dt + \frac{1}{\sqrt{P}} \int_0^T n(t)g_{x_i}^*(t)dt \quad (3.38)$$

$$= \tilde{h}\sqrt{P} + n_m \quad (3.39)$$

Under hypothesis $x_i = -1$

$$\mathbf{r} = \begin{bmatrix} r_{-1} \\ r_{+1} \end{bmatrix} = \begin{bmatrix} \sqrt{P\tilde{h}} \\ 0 \end{bmatrix} + \begin{bmatrix} n_{-1} \\ n_{+1} \end{bmatrix} \sim \mathcal{CN} \left(\underbrace{\begin{bmatrix} \sqrt{P\tilde{h}} \\ 0 \end{bmatrix}}_{\boldsymbol{\mu}_{-1}}, \underbrace{\mathbf{I}_2}_{\mathbf{C}} \right) \quad (3.40)$$

and for the noise component

$$\begin{bmatrix} n_{-1} \\ n_{+1} \end{bmatrix} \sim \mathcal{CN}(\mathbf{0}_{2 \times 1}, \mathbf{I}_2) \quad (3.41)$$

The Probability density function (PDF) for complex normal distribution in this case can be computed as

$$f_{\mathbf{r}|x_i=-1}(\mathbf{r}) = \frac{1}{\pi^2} \exp \left(- \left(|r_{-1}|^2 - r_{-1}^* \sqrt{P\tilde{h}} - r_{-1} \sqrt{P\tilde{h}}^* + |\tilde{h}|^2 P + |r_{+1}|^2 \right) \right) \quad (3.42)$$

The proof can be found at B.8. Similarly, under hypothesis $x_i = +1$

$$\mathbf{r} = \begin{bmatrix} r_{-1} \\ r_{+1} \end{bmatrix} = \begin{bmatrix} 0 \\ \sqrt{P\tilde{h}} \end{bmatrix} + \begin{bmatrix} n_{-1} \\ n_{+1} \end{bmatrix} \sim \mathcal{CN} \left(\underbrace{\begin{bmatrix} 0 \\ \sqrt{P\tilde{h}} \end{bmatrix}}_{\boldsymbol{\mu}_{+1}}, \underbrace{\mathbf{I}_2}_{\mathbf{C}} \right) \quad (3.43)$$

for

$$\begin{bmatrix} n_{-1} \\ n_{+1} \end{bmatrix} \sim \mathcal{CN}(\mathbf{0}_{2 \times 1}, \mathbf{I}_2) \quad (3.44)$$

and

$$f_{\mathbf{r}|x_i=+1}(\mathbf{r}) = \frac{1}{\pi^2} \exp \left(- \left(|r_{-1}|^2 + |r_{+1}|^2 - r_{+1}^* \sqrt{P\tilde{h}} - r_{+1} \sqrt{P\tilde{h}}^* + |\tilde{h}|^2 P \right) \right) \quad (3.45)$$

Due to the fact that the transmitted symbols are equiprobable, the optimal coherent detector utilizes the ML criterion which compares the values of the conditional probability density functions $f_{\mathbf{r}|x_i=-1}(\mathbf{r})$ and $f_{\mathbf{r}|x_i=+1}(\mathbf{r})$ calculated on the received sample.

$$f_{\mathbf{r}|x_i=-1}(\mathbf{r}) \underset{\hat{x}_i=+1}{\overset{\hat{x}_i=-1}{\gtrless}} f_{\mathbf{r}|x_i=+1}(\mathbf{r}) \Rightarrow \text{sign} \left(\Re\{(r_{-1}^* \tilde{h})\} - \Re\{(r_{+1}^* \tilde{h})\} \right) \underset{\hat{x}_i=+1}{\overset{\hat{x}_i=-1}{\gtrless}} 0 \quad (3.46)$$

For a proof check B.9.

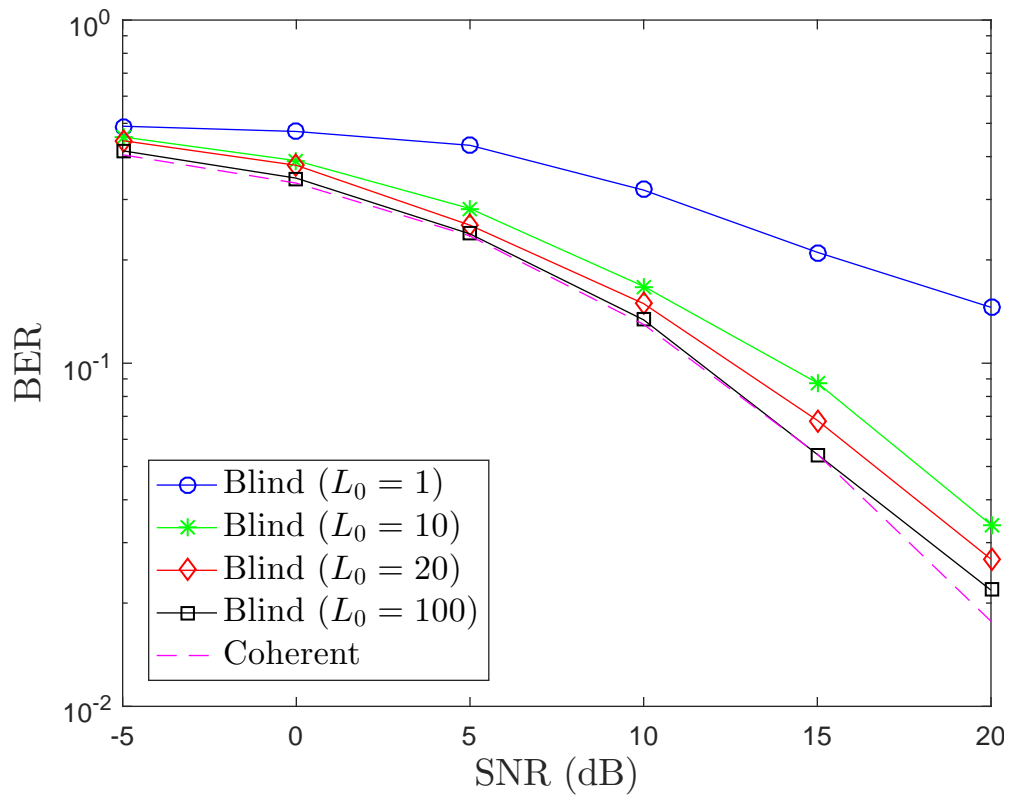


Figure 3.4: Bit error rate versus SNR of detection in BFSK.

OQPSK Appendix

A.1 Likelihood derivation

$$\frac{1}{N_0} \int_{T_0} [r(t) - s(t; \boldsymbol{\theta})]^2 dt = \frac{1}{N_0} \int_{T_0} \left[\sum_{n=1}^N (r_n - s_n(\boldsymbol{\theta})) \phi_n(t) \right]^2 dt \quad (\text{A.1})$$

$$= \frac{1}{N_0} \int_{T_0} \sum_{n=1}^N \sum_{m=1}^N (r_n - s_n(\boldsymbol{\theta})) (r_m - s_m(\boldsymbol{\theta})) \phi_n(t) \phi_m(t) dt \quad (\text{A.2})$$

$$= \frac{1}{N_0} \int_{T_0} \sum_{n=1}^N \sum_{m=1}^N (r_n - s_n(\boldsymbol{\theta})) (r_m - s_m(\boldsymbol{\theta})) \delta_{mn} dt \quad (\text{A.3})$$

$$= \frac{1}{N_0} \int_{T_0} \sum_{n=1}^N (r_n - s_n(\boldsymbol{\theta})) (r_n - s_n(\boldsymbol{\theta})) dt \quad (\text{A.4})$$

$$= \frac{1}{2\sigma^2} \int_{T_0} \sum_{n=1}^N [r_n - s_n(\boldsymbol{\theta})]^2 dt \quad (\text{A.5})$$

where in (A.3) the orthonormality condition of the basis functions demands that: $\int_{T_0} \phi_n(t) \phi_m(t) dt = \delta_{mn}$ and $\sigma^2 = N_0/2$.

A.2 CLF general form

$$\Lambda(\mathbf{a}, \mathbf{b}, h, \theta, \tau) = 2h \Re \left\{ e^{-j\theta} \int_0^{T_0} r(t) s^*(t - \tau) dt \right\} - h^2 \int_0^{T_0} |s(t - \tau)|^2 dt \quad (\text{A.6})$$

$$= 2h \Re \left\{ e^{-j\theta} \left| \int_0^{T_0} r(t) s^*(t - \tau) dt \right| e^{j\vartheta(\mathbf{a}, \mathbf{b}, \tau)} \right\} - h^2 \int_0^{T_0} |s(t - \tau)|^2 dt \quad (\text{A.7})$$

$$= 2h \left| \int_0^{T_0} r(t) s^*(t - \tau) dt \right| \Re \left\{ e^{-j(\theta - \vartheta(\mathbf{a}, \mathbf{b}, \tau))} \right\} - h^2 \int_0^{T_0} |s(t - \tau)|^2 dt \quad (\text{A.8})$$

$$= 2h \left| \int_0^{T_0} r(t) s^*(t - \tau) dt \right| \cos(-(\theta - \vartheta(\mathbf{a}, \mathbf{b}, \tau))) - h^2 \int_0^{T_0} |s(t - \tau)|^2 dt \quad (\text{A.9})$$

A.3 Limits of the likelihood

First of all we need to make clear that the SRRC pulse, as defined in (2.3), is nonzero only in the interval $[0, D_g T)$. For the proof we can take the summation terms that correspond to values of the index that are one unit less or more than the defined limits. Thus, for $i = -D_g - 1$ the integral of (2.31) becomes

$$X_i(\tau) \Big|_{i=-D_g-1} = \int_0^{T_0} r(t)g(t - \tau - (-D_g - 1)T)dt \quad (\text{A.10})$$

$$= \int_{-\tau - (-D_g - 1)T}^{T_0 - \tau - (-D_g - 1)T} r(t' + \tau + (-D_g - 1)T)g(t')dt' \quad (\text{A.11})$$

by setting $t' = t - \tau - (-D_g - 1)T$. We can see that the range of integration in (A.11) and the domain of $g(t)$ do not overlap if the following condition is met

$$-\tau - (-D_g - 1)T > D_g T \Leftrightarrow \tau < T \quad (\text{A.12})$$

Similarly the integral in (2.32) is

$$X_{i+1/2}(\tau) \Big|_{i=-D_g-1} = \int_0^{T_0} r(t)g(t - \tau - T/2 - (-D_g - 1)T)dt \quad (\text{A.13})$$

$$= \int_{-\tau - T/2 - (-D_g - 1)T}^{T_0 - \tau - T/2 - (-D_g - 1)T} r(t' + \tau + T/2 + (-D_g - 1)T)g(t')dt' \quad (\text{A.14})$$

by setting $t' = t - \tau - T/2 - (-D_g - 1)T$. The integral's range in (A.14) and the domain of $g(t)$ do not overlap if

$$-\tau - T/2 - (-D_g - 1)T > D_g T \Leftrightarrow \tau < T/2 \quad (\text{A.15})$$

From (A.12) and (A.15) we demand that $\tau < T/2$. This is a reasonable assumption that emerges from the fact that the order of transmission of the in-phase and the quadrature components can be interchanged.

We also have that

$$X_i(\tau) \Big|_{i=L_0} = \int_0^{T_0} r(t)g(t - \tau - L_0 T)dt \quad (\text{A.16})$$

$$= \int_{-\tau - L_0 T}^{T_0 - \tau - L_0 T} r(t' + \tau + L_0 T)g(t')dt' \quad (\text{A.17})$$

$$= \int_{-\tau - L_0 T}^{-\tau} r(t' + \tau + L_0 T)g(t')dt' \quad (\text{A.18})$$

by setting $t' = t - \tau - L_0 T$. This expression is zero for $\tau > 0$. Also

$$X_{i+1/2}(\tau) \Big|_{i=L_0} = \int_0^{T_0} r(t)g(t - \tau - T/2 - L_0 T)dt \quad (\text{A.19})$$

$$= \int_{-\tau-T/2-L_0T}^{T_0-\tau-T/2-L_0T} r(t' + \tau + T/2 + L_0T)g(t')dt' \quad (\text{A.20})$$

$$= \int_{-\tau-T/2-L_0T}^{-\tau-T/2} r(t' + \tau + T/2 + L_0T)g(t')dt' \quad (\text{A.21})$$

by setting $t' = t - \tau - T/2 - L_0T$. This expression is zero for $\tau > -T/2$. Both of these are assumptions of the signal model. The above derivation leads us to the conclusion that the summations in the likelihood of (2.30) are zero $\forall i < -D_g$ and $\forall i > L_0 - 1$.

A.4 Mackenthun's maximization with respect to angle

$$\max_{\mathbf{d} \in \{\pm 1\}^{N+1}} |\mathbf{d}^T \mathbf{y}| = \max_{\mathbf{d} \in \{\pm 1\}^{N+1}} |d_0 y_0 + d_1 y_1 + \dots + d_N y_N| \quad (\text{A.22})$$

$$= \max_{\mathbf{d} \in \{\pm 1\}^{N+1}} |z| \quad (\text{A.23})$$

$$= \max_{\mathbf{d} \in \{\pm 1\}^{N+1}} |z| \max_{\phi \in [0, 2\pi)} \cos(-(\phi - \vartheta_z)) \quad (\text{A.24})$$

$$= \max_{\mathbf{d} \in \{\pm 1\}^{N+1}} |z| \max_{\phi \in [0, 2\pi)} \Re \left\{ e^{-j(\phi - \vartheta_z)} \right\} \quad (\text{A.25})$$

$$= \max_{\mathbf{d} \in \{\pm 1\}^{N+1}} \max_{\phi \in [0, 2\pi)} \Re \left\{ e^{-j\phi} |z| e^{j\vartheta_z} \right\} \quad (\text{A.26})$$

$$= \max_{\mathbf{d} \in \{\pm 1\}^{N+1}} \max_{\phi \in [0, 2\pi)} \Re \left\{ e^{-j\phi} (d_0 y_0 + d_1 y_1 + \dots + d_N y_N) \right\} \quad (\text{A.27})$$

$$= \max_{\phi \in [0, 2\pi)} \max_{\mathbf{d} \in \{\pm 1\}^{N+1}} \left\{ d_0 \Re \left\{ e^{-j\phi} y_0 \right\} + d_1 \Re \left\{ e^{-j\phi} y_1 \right\} + \dots \right. \\ \left. \dots + d_N \Re \left\{ e^{-j\phi} y_N \right\} \right\} \quad (\text{A.28})$$

for $z = d_0 y_0 + d_1 y_1 + \dots + d_N y_N$ and $\vartheta_z = \arg \{z\}$.

A.5 CLF maximization equivalent problem

$$\left| \sum_{k=0}^{2(L_0+D_g)-1} c_k^* y_k \right|^2 = \left| c_0^* y_0 + c_1^* y_1 + \dots + c_{2(L_0+D_g)-1}^* y_{2(L_0+D_g)-1} \right|^2 \quad (\text{A.29})$$

$$= \left| a_{-D_g} X_{-D_g}(\tau) + b_{-D_g} (-j X_{-D_g+1/2}(\tau)) + \dots \right. \\ \left. \dots + a_{L_0-1} X_{L_0-1}(\tau) + b_{L_0-1} (-j X_{L_0-1+1/2}(\tau)) \right|^2 \quad (\text{A.30})$$

$$= \left| a_{-D_g} X_{-D_g}(\tau) + \dots + a_{L_0-1} X_{L_0-1}(\tau) - \dots \right. \\ \left. \dots - j \left[b_{-D_g} (X_{-D_g+1/2}(\tau)) + b_{L_0-1} (X_{L_0-1+1/2}(\tau)) \right] \right|^2 \quad (\text{A.31})$$

$$= \left| \sum_{i=-D_g}^{L_0-1} a_i X_i(\tau) - j \sum_{i=-D_g}^{L_0-1} b_i X_{i+1/2}(\tau) \right|^2 \quad (\text{A.32})$$

A.6 CLF periodicity proof

$$\Lambda(\tau + T/2) = \left| \sum_{i=-D_g}^{L_0-1} \hat{a}_i(\tau + \frac{T}{2}) X_i(\tau + \frac{T}{2}) - j \sum_{i=-D_g}^{L_0-1} \hat{b}_i(\tau + \frac{T}{2}) X_{i+1/2}(\tau + \frac{T}{2}) \right|^2 \quad (\text{A.33})$$

$$= \left| \sum_{i=-D_g}^{L_0-1} -\hat{b}_i(\tau) X_i(\tau + \frac{T}{2}) - j \sum_{i=-D_g}^{L_0-1} -\hat{a}_{i+1}(\tau) X_{i+1/2}(\tau + \frac{T}{2}) \right|^2 \quad (\text{A.34})$$

$$= \left| \sum_{i=-D_g}^{L_0-1} -\hat{b}_i(\tau) X_{i+1/2}(\tau) + j \sum_{i=-D_g}^{L_0-1} \hat{a}_{i+1}(\tau) X_{i+1}(\tau) \right|^2 \quad (\text{A.35})$$

$$= \left| jY(\tau) - \hat{a}_{-D_g}(\tau) X_{-D_g}(\tau) \right|^2 \quad (\text{A.36})$$

$$\approx |Y(\tau)|^2 \quad (\text{A.37})$$

$$= \Lambda(\tau) \quad (\text{A.38})$$

where for (A.35) we take the absolute value of the complex conjugate and in (A.37) it is reasonable to assume that for large observation intervals the contribution of a term to the metric is negligible.

A.7 Equivalent correlation of angles in the frequency domain

$$(2.59) \stackrel{(2.62)}{\Leftrightarrow} \Im \left\{ \left(\int r^*(t)g(t - \tau - (-D_g + i/2)T)dt \right) \cdot \left(\int r(t)g(t - \tau - (-D_g + k/2)T)dt \right) \right\} = 0 \quad (\text{A.39})$$

$$\Leftrightarrow \Im \left\{ \int \left(\int (r^*(t_1)g(t_1 - \tau - (-D_g + i/2)T) \cdot r(t_2)g(t_2 - \tau - (-D_g + k/2)T)) dt_1 \right) dt_2 \right\} = 0 \quad (\text{A.40})$$

$$\Leftrightarrow \int \left(\int (\Im \{ r^*(t_1)r(t_2) \} g(t_1 - \tau - (-D_g + i/2)T) \cdot g(t_2 - \tau - (-D_g + k/2)T)) dt_1 \right) dt_2 = 0 \quad (\text{A.41})$$

$$\Leftrightarrow \int \left(\int (r(t_1, t_2)g^*(t_1 - \tau - (-D_g + i/2)T, t_2 - \tau - (-D_g + k/2)T)) dt_1 \right) dt_2 = 0 \quad (\text{A.42})$$

$$\Leftrightarrow \int \left(\int (R(F_1, F_2)G_{T_0}^*(F_1, F_2) \cdot e^{-j2\pi(F_1(\tau + (-D_g + i/2)T) + F_2(\tau + (-D_g + k/2)T))}) dt_1 \right) dt_2 = 0 \quad (\text{A.43})$$

where we have defined the following quantities

$$g(t_1 - x)g(t_2 - y) = g(t_1 - x, t_2 - y), \quad x, y \in \mathbb{R} \quad (\text{A.44})$$

$$R(F_1, F_2) = \mathcal{F} \{ r(t_1, t_2) \} \quad (\text{A.45})$$

$$G_{T_0}(F_1, F_2) = \mathcal{F} \{g_{T_0}(t_1, t_2)\} = \mathcal{F} \{g_{T_0}(t_1)g_{T_0}(t_2)\} \quad (\text{A.46})$$

$$g_{T_0}(t_i) = \begin{cases} g(t_i), & 0 \leq t_i \leq T_0 \\ -1, & \text{otherwise} \end{cases} \quad (\text{A.47})$$

and (A.42) is because the signalling pulse $g(t)$ is real while 2D Parseval's theorem proven in A.9 and 2D shifting property proved in A.10 leads to (A.43).

A.8 CLF simplified form

$$\Lambda(\tau) = \left| \sum_{i=-D_g}^{L_0-1} \hat{a}_i(\tau)X_i(\tau) - j \sum_{i=-D_g}^{L_0-1} \hat{b}_i(\tau)X_{i+1/2}(\tau) \right|^2 \quad (\text{A.48})$$

$$= \left[\sum_{i=-D_g}^{L_0-1} \hat{a}_i(\tau)X_i(\tau) - j \sum_{i=-D_g}^{L_0-1} \hat{b}_i(\tau)X_{i+1/2}(\tau) \right] \cdot \left[\sum_{i=-D_g}^{L_0-1} \hat{a}_i(\tau)X_i(\tau) - j \sum_{i=-D_g}^{L_0-1} \hat{b}_i(\tau)X_{i+1/2}(\tau) \right]^* \quad (\text{A.49})$$

$$\begin{aligned} &= \sum_{i=-D_g}^{L_0-1} \left\{ \sum_{k=-D_g}^{L_0-1} \{ \hat{a}_i(\tau)X_i(\tau)\hat{a}_k(\tau)X_k^*(\tau) \} \right\} \\ &\quad + j \sum_{i=-D_g}^{L_0-1} \left\{ \sum_{k=-D_g}^{L_0-1} \{ \hat{a}_i(\tau)X_i(\tau)\hat{b}_k(\tau)X_{k+1/2}^*(\tau) \} \right\} \\ &\quad - j \sum_{i=-D_g}^{L_0-1} \left\{ \sum_{k=-D_g}^{L_0-1} \{ \hat{b}_i(\tau)X_{i+1/2}(\tau)\hat{a}_k(\tau)X_k^*(\tau) \} \right\} \\ &\quad + \sum_{i=-D_g}^{L_0-1} \left\{ \sum_{k=-D_g}^{L_0-1} \{ \hat{b}_i(\tau)X_{i+1/2}(\tau)\hat{b}_k(\tau)X_{k+1/2}^*(\tau) \} \right\} \end{aligned} \quad (\text{A.50})$$

A.9 2D Parseval's theorem

Suppose we have two two-dimensional 2D signals, then their time representation with respect to their equivalents in the frequency domain would be

$$x(t_1, t_2) = \int \int X(F_1, F_2)e^{j2\pi(F_1t_1+F_2t_2)}dF_1dF_2 \quad (\text{A.51})$$

$$y(t_1, t_2) = \int \int Y(F_1, F_2)e^{j2\pi(F_1t_1+F_2t_2)}dF_1dF_2 \quad (\text{A.52})$$

Subsequently

$$\int \int x(t_1, t_2)y^*(t_1, t_2)dt_1dt_2 \quad (\text{A.53})$$

$$= \int \int \left[\left(\int \int X(F_1, F_2)e^{j2\pi(F_1t_1+F_2t_2)}dF_1dF_2 \right) \left(\int \int Y(F_1, F_2)e^{j2\pi(F_1t_1+F_2t_2)}dF_1dF_2 \right)^* \right] dt_1dt_2 \quad (\text{A.54})$$

$$= \iint \left[\iint \left(\iint X(F_1, F_2) e^{j2\pi(F_1 t_1 + F_2 t_2)} Y^*(F_3, F_4) e^{-j2\pi(F_3 t_1 + F_4 t_2)} dF_1 dF_2 \right) dF_3 dF_4 \right] dt_1 dt_2 \quad (\text{A.55})$$

$$= \iint \left[\iint \left(\iint X(F_1, F_2) Y^*(F_3, F_4) e^{j2\pi((F_1 - F_3)t_1 + (F_2 - F_4)t_2)} dF_1 dF_2 \right) dF_3 dF_4 \right] dt_1 dt_2 \quad (\text{A.56})$$

$$= \iint \left[\iint \left(\iint X(F_1, F_2) Y^*(F_3, F_4) e^{j2\pi((F_1 - F_3)t_1 + (F_2 - F_4)t_2)} dt_1 dt_2 \right) dF_1 dF_2 \right] dF_3 dF_4 \quad (\text{A.57})$$

$$= \iint \left[\iint \left(X(F_1, F_2) Y^*(F_3, F_4) \int \int 1 \cdot e^{j2\pi((F_1 - F_3)t_1 + (F_2 - F_4)t_2)} dt_1 dt_2 \right) dF_1 dF_2 \right] dF_3 dF_4 \quad (\text{A.58})$$

$$= \iint \left[\iint \left(X(F_1, F_2) Y^*(F_3, F_4) \delta(F_1 - F_3, F_2 - F_4) \right) dF_1 dF_2 \right] dF_3 dF_4 \quad (\text{A.59})$$

$$= \iint X(F_3, F_4) Y^*(F_3, F_4) dF_3 dF_4 \quad (\text{A.60})$$

$$= \iint X(F_1, F_2) Y^*(F_1, F_2) dF_1 dF_2 \quad (\text{A.61})$$

where for (A.59) the 2D delta function is defined as

$$\mathcal{F}\{\delta(t_1, t_2)\} = \int \int \delta(t_1, t_2) e^{-j2\pi(F_1 t_1 + F_2 t_2)} dt_1 dt_2 = e^{-j2\pi(F_1 \cdot 0 + F_2 \cdot 0)} = 1 \quad (\text{A.62})$$

and

$$\mathcal{F}^{-1}\{\delta(F_1, F_2)\} = \int \int \delta(F_1, F_2) e^{j2\pi(F_1 t_1 + F_2 t_2)} dF_1 dF_2 = e^{-j2\pi(0 \cdot t_1 + 0 \cdot t_2)} = 1 \quad (\text{A.63})$$

and for (A.60) we resort to the 2D sampling property.

A.10 2D frequency shifting property

$$\mathcal{F}\{x(t_1 - a, t_2 - b)\} = \int \int x(t_1 - a, t_2 - b) e^{-j2\pi(F_1 t_1 + F_2 t_2)} dt_1 dt_2 \quad (\text{A.64})$$

$$\stackrel{\substack{t'_1 \leftarrow t_1 - a \\ t'_2 \leftarrow t_2 - b}}{=} \int \int x(t'_1, t'_2) e^{-j2\pi(F_1(t'_1 + a) + F_2(t'_2 + b))} dt'_1 dt'_2 \quad (\text{A.65})$$

$$= \int \int x(t'_1, t'_2) e^{-j2\pi(F_1 t'_1 + F_2 t'_2)} e^{-j2\pi(F_1 a + F_2 b)} dt'_1 dt'_2 \quad (\text{A.66})$$

$$\stackrel{\substack{t_1 \leftarrow t'_1 \\ t_2 \leftarrow t'_2}}{=} e^{-j2\pi(F_1 a + F_2 b)} \int \int x(t_1, t_2) e^{-j2\pi(F_1 t_1 + F_2 t_2)} dt_1 dt_2 \quad (\text{A.67})$$

$$= e^{-j2\pi(F_1 a + F_2 b)} X(F_1, F_2) \quad (\text{A.68})$$

FSK Appendix

B.1 Likelihood form

$$\Lambda(\mathbf{x}, \tau) = \left| \int_0^{T_0} r(t) s^*(t - \tau) dt \right|^2 \quad (\text{B.1})$$

$$= \left| \int_0^{T_0} r(t) \left[\sum_{i=-1}^{L_0-1} \sqrt{\frac{P}{T}} e^{-j2\pi F_{x_i}(t-\tau-iT)} u_T(t - \tau - iT) \right] dt \right|^2 \quad (\text{B.2})$$

$$= \left| \sum_{i=-1}^{L_0-1} \left\{ \int_0^{T_0} r(t) \sqrt{\frac{P}{T}} e^{-j2\pi F_{x_i}(t-\tau-iT)} u_T(t - \tau - iT) dt \right\} \right|^2 \quad (\text{B.3})$$

$$= \left| \sum_{i=-1}^{L_0-1} \left\{ \frac{x_i - 1}{2} \int_0^{T_0} -r(t) \sqrt{\frac{P}{T}} e^{-j2\pi F_{-1}(t-\tau-iT)} u_T(t - \tau - iT) dt + \dots \right. \right. \\ \left. \left. \dots + \frac{x_i + 1}{2} \int_0^{T_0} r(t) \sqrt{\frac{P}{T}} e^{-j2\pi F_1(t-\tau-iT)} u_T(t - \tau - iT) dt \right\} \right|^2 \quad (\text{B.4})$$

$$= \left| \sum_{i=-1}^{L_0-1} \left\{ x_i \int_0^{T_0} -\frac{r(t)}{2} \sqrt{\frac{P}{T}} e^{-j2\pi F_{-1}(t-\tau-iT)} u_T(t - \tau - iT) dt + \dots \right. \right. \\ \left. \left. \dots + \int_0^{T_0} -\frac{r(t)}{2} \sqrt{\frac{P}{T}} e^{-j2\pi F_{-1}(t-\tau-iT)} u_T(t - \tau - iT) dt + \dots \right. \right. \\ \left. \left. \dots + x_i \int_0^{T_0} \frac{r(t)}{2} \sqrt{\frac{P}{T}} e^{-j2\pi F_1(t-\tau-iT)} u_T(t - \tau - iT) dt + \dots \right. \right. \\ \left. \left. \dots + \int_0^{T_0} \frac{r(t)}{2} \sqrt{\frac{P}{T}} e^{-j2\pi F_1(t-\tau-iT)} u_T(t - \tau - iT) dt \right\} \right|^2 \quad (\text{B.5})$$

$$= \left| \sum_{i=-1}^{L_0-1} \left\{ x_i \left[\int_0^{T_0} \frac{r(t)}{2} \sqrt{\frac{P}{T}} e^{-j2\pi F_1(t-\tau-iT)} u_T(t - \tau - iT) dt - \dots \right. \right. \right.$$

$$\begin{aligned}
& \left. \dots - \int_0^{T_0} \frac{r(t)}{2} \sqrt{\frac{P}{T}} e^{-j2\pi F_{-1}(t-\tau-iT)} u_T(t-\tau-iT) dt \right] \Big\} + \dots \\
& \dots + \sum_{i=-1}^{L_0-1} \left\{ \int_0^{T_0} \frac{r(t)}{2} \sqrt{\frac{P}{T}} e^{-j2\pi F_{-1}(t-\tau-iT)} u_T(t-\tau-iT) dt + \dots \right. \\
& \quad \left. \dots + \int_0^{T_0} \frac{r(t)}{2} \sqrt{\frac{P}{T}} e^{-j2\pi F_1(t-\tau-iT)} u_T(t-\tau-iT) dt \right\}^2 \tag{B.6}
\end{aligned}$$

The proof for the limits of the CLF's summation is in B.10.

B.2 Maximization algorithm's input

$$y_{i+1} = \begin{cases} \int_0^{T_0} \frac{r(t)}{2} \sqrt{\frac{P}{T}} e^{-j2\pi F_1(t-\tau-iT)} u_T(t-\tau-iT) dt - \dots \\ \dots - \int_0^{T_0} \frac{r(t)}{2} \sqrt{\frac{P}{T}} e^{-j2\pi F_{-1}(t-\tau-iT)} u_T(t-\tau-iT) dt, & i = -1, 0, \dots, L_0 - 1 \\ \sum_{a=-1}^{L_0-1} \left\{ \int_0^{T_0} \frac{r(t)}{2} \sqrt{\frac{P}{T}} e^{-j2\pi F_{-1}(t-\tau-aT)} u_T(t-\tau-aT) dt + \dots \right. \\ \quad \left. \dots + \int_0^{T_0} \frac{r(t)}{2} \sqrt{\frac{P}{T}} e^{-j2\pi F_1(t-\tau-aT)} u_T(t-\tau-aT) dt \right\}, & i = L_0 \end{cases} \tag{B.7}$$

$$= \begin{cases} \frac{1}{2} \sqrt{\frac{P}{T}} \left[\int_0^{T_0} r(t) e^{-j2\pi F_1(t-\tau-iT)} u_T(t-\tau-iT) dt - \dots \right. \\ \quad \left. \dots - \int_0^{T_0} r(t) e^{-j2\pi F_{-1}(t-\tau-iT)} u_T(t-\tau-iT) dt \right], & i = -1, 0, \dots, L_0 - 1 \\ \sum_{a=-1}^{L_0-1} \left\{ \frac{1}{2} \sqrt{\frac{P}{T}} \left[\int_0^{T_0} r(t) e^{-j2\pi F_{-1}(t-\tau-aT)} u_T(t-\tau-aT) dt + \dots \right. \right. \\ \quad \left. \left. \dots + \int_0^{T_0} r(t) e^{-j2\pi F_1(t-\tau-aT)} u_T(t-\tau-aT) dt \right] \right\}, & i = L_0 \end{cases} \tag{B.8}$$

$$= \begin{cases} \frac{1}{2} \sqrt{\frac{P}{T}} \int_0^{T_0} r(t) \left[e^{-j2\pi F_1(t-\tau-iT)} - e^{-j2\pi F_{-1}(t-\tau-iT)} \right] u_T(t-\tau-iT) dt, & i = -1, 0, \dots, L_0 - 1 \\ \sum_{a=-1}^{L_0-1} \left\{ \frac{1}{2} \sqrt{\frac{P}{T}} \int_0^{T_0} r(t) \left[e^{-j2\pi F_{-1}(t-\tau-aT)} + e^{-j2\pi F_1(t-\tau-aT)} \right] u_T(t-\tau-aT) dt \right\}, & i = L_0 \end{cases} \tag{B.9}$$

B.3 Angles' correlation case 1

$$(3.15) \stackrel{(3.14)}{\Leftrightarrow} \mathfrak{S} \left\{ \left[\frac{1}{2} \sqrt{\frac{P}{T}} \int_0^{T_0} r^*(t) \left[e^{j2\pi F_1(t-\tau-iT)} - e^{j2\pi F_{-1}(t-\tau-iT)} \right] u_T(t-\tau-iT) dt \right] \right\}.$$

$$\left\{ \left[\frac{1}{2} \sqrt{\frac{P}{T}} \int_0^{T_0} r(t) \left[e^{-j2\pi F_1(t-\tau-kT)} - e^{-j2\pi F_{-1}(t-\tau-kT)} \right] u_T(t-\tau-kT) dt \right] \right\} = 0 \quad (\text{B.10})$$

$$\Leftrightarrow \Im \left\{ \left[\int_0^{T_0} r^*(t) \left[e^{j2\pi F_1(t-\tau-iT)} - e^{j2\pi F_{-1}(t-\tau-iT)} \right] u_T(t-\tau-iT) dt \right] \cdot \left[\int_0^{T_0} r(t) \left[e^{-j2\pi F_1(t-\tau-kT)} - e^{-j2\pi F_{-1}(t-\tau-kT)} \right] u_T(t-\tau-kT) dt \right] \right\} = 0 \quad (\text{B.11})$$

$$\Leftrightarrow \int_0^{T_0} \left(\int_0^{T_0} \left(\Im \left\{ r^*(t_1) r(t_2) \left[e^{j2\pi F_1(t_1-\tau-iT)} - e^{j2\pi F_{-1}(t_1-\tau-iT)} \right] \cdot \left[e^{-j2\pi F_1(t_2-\tau-kT)} - e^{-j2\pi F_{-1}(t_2-\tau-kT)} \right] \right\} \right) u_T(t_1-\tau-iT) u_T(t_2-\tau-kT) dt_1 \right) dt_2 = 0 \quad (\text{B.12})$$

$$\Leftrightarrow \int_0^{T_0} \left(\int_0^{T_0} \left(R(F_a, F_b) e^{-j2\pi(F_a(\tau+iT)+F_b(\tau+kT))} \cdot G^*(F_a, F_b) e^{-j2\pi(F_a(\tau+iT)+F_b(\tau+kT))} \right) dF_a \right) dF_b = 0 \quad (\text{B.13})$$

$$\Leftrightarrow \int_0^{T_0} \left(\int_0^{T_0} \left(R(F_a, F_b) G^*(F_a, F_b) e^{-j4\pi(F_a(\tau+iT)+F_b(\tau+kT))} \right) dF_a \right) dF_b = 0 \quad (\text{B.14})$$

B.4 Angles' correlation case 2

$$(3.15) \stackrel{(3.14)}{\Leftrightarrow} \Im \left\{ \left[\frac{1}{2} \sqrt{\frac{P}{T}} \int_0^{T_0} r^*(t) \left[e^{j2\pi F_1(t-\tau-iT)} - e^{j2\pi F_{-1}(t-\tau-iT)} \right] u_T(t-\tau-iT) dt \right] \cdot \left[\sum_{a=-1}^{L_0-1} \left\{ \frac{1}{2} \sqrt{\frac{P}{T}} \int_0^{T_0} r(t) \left[e^{-j2\pi F_{-1}(t-\tau-aT)} + e^{-j2\pi F_1(t-\tau-aT)} \right] u_T(t-\tau-aT) dt \right\} \right] \right\} = 0 \quad (\text{B.15})$$

$$\Leftrightarrow \Im \left\{ \left[\int_0^{T_0} r^*(t) \left[e^{j2\pi F_1(t-\tau-iT)} - e^{j2\pi F_{-1}(t-\tau-iT)} \right] u_T(t-\tau-iT) dt \right] \cdot \left[\sum_{a=-1}^{L_0-1} \left\{ \int_0^{T_0} r(t) \left[e^{-j2\pi F_{-1}(t-\tau-aT)} + e^{-j2\pi F_1(t-\tau-aT)} \right] u_T(t-\tau-aT) dt \right\} \right] \right\} = 0 \quad (\text{B.16})$$

$$\Leftrightarrow \sum_{a=-1}^{L_0-1} \left\{ \int_0^{T_0} \left(\int_0^{T_0} \left(\Im \left\{ r^*(t_1) r(t_2) \left[e^{j2\pi F_1(t_1-\tau-iT)} - e^{j2\pi F_{-1}(t_1-\tau-iT)} \right] \right\} \right) \right) dt_1 \right\} dt_2 = 0$$

$$= \left| \int_0^{T_0} r(t) \sum_{i=-1}^{L_0-1} \left\{ e^{-j2\pi F_1(t-iT)} u_T(t-\tau-iT) \right\} dt \right|^2 \quad (\text{B.24})$$

in which the summation is a sum over non-overlapping parts of a signal integrated on the same interval each time for any value of τ and thus remains unchanged given that $\tau \ll T_0$.

B.6 Alternative likelihood

$$\Lambda_2(\tau) = \left| \sum_{i=-1}^{L_0-1} \left\{ \int_0^{T_0} \frac{r(t)}{2} \sqrt{\frac{P}{T}} e^{-j2\pi F_1(t-\tau-iT)} u_T(t-\tau-iT) dt + \dots \right. \right. \\ \left. \left. \dots + \int_0^{T_0} \frac{r(t)}{2} \sqrt{\frac{P}{T}} e^{-j2\pi F_1(t-\tau-iT)} u_T(t-\tau-iT) dt \right\} \right|^2 \quad (\text{B.25})$$

$$= \left[\sum_{i=-1}^{L_0-1} \left\{ \int_0^{T_0} \frac{r(t)}{2} \sqrt{\frac{P}{T}} e^{-j2\pi F_1(t-\tau-iT)} u_T(t-\tau-iT) dt + \dots \right. \right. \\ \left. \left. \dots + \int_0^{T_0} \frac{r(t)}{2} \sqrt{\frac{P}{T}} e^{-j2\pi F_1(t-\tau-iT)} u_T(t-\tau-iT) dt \right\} \right] \\ \left[\sum_{i=-1}^{L_0-1} \left\{ \int_0^{T_0} \frac{r(t)}{2} \sqrt{\frac{P}{T}} e^{-j2\pi F_1(t-\tau-iT)} u_T(t-\tau-iT) dt + \dots \right. \right. \\ \left. \left. \dots + \int_0^{T_0} \frac{r(t)}{2} \sqrt{\frac{P}{T}} e^{-j2\pi F_1(t-\tau-iT)} u_T(t-\tau-iT) dt \right\} \right]^* \quad (\text{B.26})$$

$$= \sum_{i=-1}^{L_0-1} \left\{ \sum_{k=-1}^{L_0-1} \left\{ \left[\int_0^{T_0} \frac{r(t)}{2} \sqrt{\frac{P}{T}} e^{-j2\pi F_1(t-\tau-iT)} u_T(t-\tau-iT) dt + \dots \right. \right. \right. \\ \left. \left. \dots + \int_0^{T_0} \frac{r(t)}{2} \sqrt{\frac{P}{T}} e^{-j2\pi F_1(t-\tau-iT)} u_T(t-\tau-iT) dt \right] \right. \\ \left. \left[\int_0^{T_0} \frac{r^*(t)}{2} \sqrt{\frac{P}{T}} e^{j2\pi F_1(t-\tau-kT)} u_T(t-\tau-kT) dt + \dots \right. \right. \\ \left. \left. \dots + \int_0^{T_0} \frac{r^*(t)}{2} \sqrt{\frac{P}{T}} e^{j2\pi F_1(t-\tau-kT)} u_T(t-\tau-kT) dt \right] \right\} \quad (\text{B.27})$$

B.7 Alternative likelihood derivative

$$\frac{\vartheta I(\tau; F, i)}{\vartheta \tau} = \int_0^{T_0} r(t) \frac{\vartheta (e^{-j2\pi F(t-\tau-iT)} u_T(t-\tau-iT))}{\vartheta \tau} dt \quad (\text{B.28})$$

$$= \int_0^{T_0} r(t) \left[\frac{\vartheta(e^{-j2\pi F(t-\tau-iT)})}{\vartheta\tau} u_T(t-\tau-iT) + e^{-j2\pi F(t-\tau-iT)} \frac{\vartheta(u_T(t-\tau-iT))}{\vartheta\tau} \right] dt \quad (\text{B.29})$$

$$= \int_0^{T_0} r(t) \left[j2\pi F e^{-j2\pi F(t-\tau-iT)} u_T(t-\tau-iT) + e^{-j2\pi F(t-\tau-iT)} \frac{\vartheta(u_T(t-\tau-iT))}{\vartheta\tau} \right] dt \quad (\text{B.30})$$

$$= \int_0^{T_0} r(t) \left[j2\pi F e^{-j2\pi F(t-\tau-iT)} u_T(t-\tau-iT) + e^{-j2\pi F(t-\tau-iT)} \cdot \left(\delta(t-\tau-iT) - \delta(t-\tau-iT-T) \right) \right] dt \quad (\text{B.31})$$

$$= \int_0^{T_0} r(t) j2\pi F e^{-j2\pi F(t-\tau-iT)} u_T(t-\tau-iT) dt + r_\delta(\tau+iT) + r_\delta(\tau+iT+T) e^{-j2\pi FT} \quad (\text{B.32})$$

for

$$r_\delta(\tau) = \begin{cases} r(t), & t \in [0, T_0] \\ 0, & \text{otherwise} \end{cases} \quad (\text{B.33})$$

The equality (B.28) is due to the Leibniz's rule

$$\frac{\vartheta}{\vartheta x} \left(\int_{a(x)}^{b(x)} f(x, t) dt \right) = f(x, b(x)) \frac{\vartheta}{\vartheta x} b(x) - f(x, a(x)) \frac{\vartheta}{\vartheta x} a(x) + \int_{a(x)}^{b(x)} \frac{\vartheta}{\vartheta x} f(x, t) dt \quad (\text{B.34})$$

The derivative of the complex exponential function for (B.30) is

$$\frac{\vartheta}{\vartheta x} e^{jf(x)} = j e^{jf(x)} \frac{\vartheta}{\vartheta x} f(x) \quad (\text{B.35})$$

and for (B.31) the differentiation of a square pulse of duration T starting at $t = f(x)$ is

$$\frac{\vartheta}{\vartheta x} u_T(t - f(x)) = \frac{\vartheta}{\vartheta x} (u(t - f(x)) - \delta(t - f(x) - T)) \quad (\text{B.36})$$

$$= -\delta(t - f(x)) \frac{\vartheta}{\vartheta x} f(x) + \delta(t - f(x) - T) \frac{\vartheta}{\vartheta x} f(x) \quad (\text{B.37})$$

$$= \frac{\vartheta}{\vartheta x} f(x) [\delta(t - f(x) - T) - \delta(t - f(x))] \quad (\text{B.38})$$

B.8 Conditional PDF of received sample (hypothesis testing)

$$f_{\mathbf{r}|x_i=-1}(\mathbf{r}) = \frac{1}{\pi^2 \det C} \exp \left(- [\mathbf{r} - \boldsymbol{\mu}_{-1}]^H C^{-1} [\mathbf{r} - \boldsymbol{\mu}_{-1}] \right) \quad (\text{B.39})$$

$$= \frac{1}{\pi^2} \exp \left(- \begin{bmatrix} r_{-1} - \sqrt{P} \tilde{h} & r_1 \end{bmatrix}^* \begin{bmatrix} r_{-1} - \sqrt{P} \tilde{h} \\ r_1 \end{bmatrix} \right) \quad (\text{B.40})$$

$$= \frac{1}{\pi^2} \exp \left(- \left(r_{-1}^* r_{-1} - r_{-1}^* \sqrt{P} \tilde{h} - r_{-1} \sqrt{P} \tilde{h}^* + |\tilde{h}|^2 P + r_1^* r_1 \right) \right) \quad (\text{B.41})$$

$$= \frac{1}{\pi^2} \exp \left(- \left(|r_{-1}|^2 - r_{-1}^* \sqrt{P} \tilde{h} - r_{-1} \sqrt{P} \tilde{h}^* + |\tilde{h}|^2 P + |r_1|^2 \right) \right) \quad (\text{B.42})$$

B.9 Maximum likelihood decision rule

$$f_{\mathbf{r}|x_i=-1}(\mathbf{r}) \underset{\hat{x}_i=+1}{\overset{\hat{x}_i=-1}{\geq}} f_{\mathbf{r}|x_i=+1}(\mathbf{r}) \quad (\text{B.43})$$

$$\Rightarrow \exp \left(- \left(|r_{-1}|^2 - r_{-1}^* \sqrt{P} \tilde{h} - r_{-1} \sqrt{P} \tilde{h}^* + |\tilde{h}|^2 P + |r_1|^2 \right) \right) \underset{\hat{x}_i=+1}{\overset{\hat{x}_i=-1}{\geq}} \dots$$

$$\dots \exp \left(- \left(|r_{-1}|^2 + |r_1|^2 - r_1^* \sqrt{P} \tilde{h} - r_1 \sqrt{P} \tilde{h}^* + |\tilde{h}|^2 P \right) \right) \quad (\text{B.44})$$

$$\Rightarrow - \left(|r_{-1}|^2 - r_{-1}^* \sqrt{P} \tilde{h} - r_{-1} \sqrt{P} \tilde{h}^* + |\tilde{h}|^2 P + |r_1|^2 \right) \underset{\hat{x}_i=+1}{\overset{\hat{x}_i=-1}{\geq}} \dots$$

$$\dots - \left(|r_{-1}|^2 + |r_1|^2 - r_1^* \sqrt{P} \tilde{h} - r_1 \sqrt{P} \tilde{h}^* + |\tilde{h}|^2 P \right) \quad (\text{B.45})$$

$$\Rightarrow \sqrt{P} \left(r_{-1}^* \tilde{h} + r_{-1} \tilde{h}^* \right) \underset{\hat{x}_i=+1}{\overset{\hat{x}_i=-1}{\geq}} \sqrt{P} \left(r_{+1}^* \tilde{h} + r_{+1} \tilde{h}^* \right) \quad (\text{B.46})$$

$$\Rightarrow 2\Re\{(r_{-1}^* \tilde{h})\} \underset{\hat{x}_i=+1}{\overset{\hat{x}_i=-1}{\geq}} 2\Re\{(r_{+1}^* \tilde{h})\} \quad (\text{B.47})$$

$$\Rightarrow \text{sign} \left(\Re\{(r_{-1}^* \tilde{h})\} - \Re\{(r_{+1}^* \tilde{h})\} \right) \underset{\hat{x}_i=+1}{\overset{\hat{x}_i=-1}{\geq}} 0 \quad (\text{B.48})$$

B.10 Limits of the likelihood

Ignoring $\sqrt{\frac{P}{T}}$ multiplier we get

$$(3.1) \stackrel{(3.2)}{\Leftrightarrow} s(t) = \sum_i e^{j2\pi F_{x_i}(t-iT)} u_T(t-iT) \quad (\text{B.49})$$

$$= \sum_i \{ \cos(2\pi F_{x_i}(t-iT)) + j \sin(2\pi F_{x_i}(t-iT)) \} u_T(t-iT) \quad (\text{B.50})$$

$$= \sum_i \{ \cos(2\pi F_{x_i}(t-iT)) u_T(t-iT) \} + j \sum_i \{ \sin(2\pi F_{x_i}(t-iT)) u_T(t-iT) \} \quad (\text{B.51})$$

$$(3.6) \stackrel{(B.51)}{\Leftrightarrow} \Lambda(\mathbf{x}, \tau) = \left| \int_0^{T_0} r(t) \left[\sum_i \{ \cos(2\pi F_{x_i}(t-\tau-iT)) u_T(t-\tau-iT) \} - \dots \right. \right. \\ \left. \left. \dots - j \sum_i \{ \sin(2\pi F_{x_i}(t-\tau-iT)) u_T(t-\tau-iT) \} \right] \right|^2 \quad (\text{B.52})$$

$$= \left| \sum_i \left\{ \int_0^{T_0} r(t) \cos(2\pi F_{x_i}(t-\tau-iT)) u_T(t-\tau-iT) dt \right\} - \dots \right|^2$$

$$\dots - j \sum_i \left\{ \int_0^{T_0} r(t) \sin(2\pi F_{x_i}(t - \tau - iT)) u_T(t - \tau - iT) dt \right\}^2 \quad (\text{B.53})$$

$$= \left| \sum_i Y_i(\tau) - j \sum_i Z_i(\tau) \right|^2 \quad (\text{B.54})$$

where

$$Y_i(\tau) = \int_0^{T_0} r(t) \cos(2\pi F_{x_i}(t - \tau - iT)) u_T(t - \tau - iT) dt \quad (\text{B.55})$$

and

$$Z_i(\tau) = \int_0^{T_0} r(t) \sin(2\pi F_{x_i}(t - \tau - iT)) u_T(t - \tau - iT) dt \quad (\text{B.56})$$

We have calculated the values of $Y_i(\tau)$ and $Z_i(\tau)$ at the following indexes to verify that they are equal to zero.

For $i = -2$

$$Y_i(\tau) \Big|_{i=-2} = \int_0^{T_0} r(t) \cos(2\pi F_{x_{-2}}(t - \tau + 2T)) u_T(t - \tau + 2T) dt \quad (\text{B.57})$$

$$= \int_0^{T_0} r(t) \cos(2\pi F_{x_{-2}}(t - \tau + 2T)) u_T(t - (\tau - 2T)) dt \quad (\text{B.58})$$

with the square pulse defined as

$$u_T(t - (\tau - 2T)) = \begin{cases} 1, & \tau - 2T \leq t < \tau - T \\ 0, & \text{otherwise} \end{cases} \quad (\text{B.59})$$

Then the following hold true

$$(B.55) \stackrel{(B.59)}{\Rightarrow} Y_i(\tau) \Big|_{i=-2} = 0, \quad \forall \tau \in [0, T] \quad (\text{B.60})$$

$$(B.56) \stackrel{(B.59)}{\Rightarrow} Z_i(\tau) \Big|_{i=-2} = 0, \quad \forall \tau \in [0, T] \quad (\text{B.61})$$

In that sense, (B.55) and (B.56) are nonzero for $i \geq -1$.

Similarly for $i = L_0$

$$Y_i(\tau) \Big|_{i=L_0} = \int_0^{T_0} r(t) \cos(2\pi F_{x_{L_0}}(t - \tau - L_0T)) u_T(t - (\tau + L_0T)) dt \quad (\text{B.62})$$

with the square pulse defined as

$$u_T(t - (\tau + L_0T)) = \begin{cases} 1, & \tau + T_0 \leq t < \tau + T_0 + T \\ 0, & \text{otherwise} \end{cases} \quad (\text{B.63})$$

Then the following hold true

$$(B.55) \stackrel{(B.63)}{\Rightarrow} Y_i(\tau) \Big|_{i=L_0} = 0, \quad \forall \tau \in [0, T] \quad (\text{B.64})$$

$$(B.56) \stackrel{(B.63)}{\Rightarrow} Z_i(\tau) \Big|_{i=L_0} = 0, \quad \forall \tau \in [0, T] \quad (\text{B.65})$$

In that sense, (B.55) and (B.56) are nonzero for $i \leq L_0 - 1$.

Bibliography

- [1] A. A. D'Amico, "Efficient Maximum-Likelihood Based Clock and Phase Estimators for OQPSK Signals," *IEEE Trans. Commun.*, vol. 64, no. 4, Apr. 2016.
- [2] P. N. Alevizos, Y. Fountzoulas, G. N. Karystinos, and A. Bletsas, "Log-linear-complexity GLRT optimal noncoherent sequence detection for orthogonal and RFID-oriented modulations," *IEEE Trans. Commun.*, vol. 63, no. 7, Jul. 2015.
- [3] J. G. Proakis and M. Salehi, *Digital Communications*, 5th ed. Englewood Cliffs, NJ, USA: Prentice-Hall, Nov. 2007.
- [4] H. L. Van Trees and K. L. Bell, *Detection Estimation and Modulation Theory, Part I*, 1st Ed. New York: Wiley, Jun. 2001.
- [5] K. M. Mackenthun, "A fast algorithm for multiple-symbol differential detection of MPSK," *IEEE Trans. Commun.*, vol. 42, no. 234, Aug. 2002.
- [6] R. C. Gonzalez and R. E. Woods, *Digital Image Processing*, 3rd ed. Upper Saddle River, NJ, USA: Prentice-Hall, Aug. 2007.
- [7] A. V. Oppenheim and R. W. Schaffer, *Discrete-Time Signal Processing*, 3rd ed. Upper Saddle River, NJ, USA: Prentice-Hall, Aug. 2009.
- [8] G. M. Vitetta, U. Mengali and D. P. Taylor, "Optimal noncoherent detection of FSK signals transmitted over linearly time-selective Rayleigh fading channels," *IEEE Trans. Commun.*, vol. 45, no. 11, Aug. 2016.
- [9] S. Shembil, "M-ary FSK with Orthogonal Pulse Envelopes and its Noncoherent Detection," *International Journal of Electrical & Computer Sciences*, vol. 10, no. 6, Dec. 2010.
- [10] A. Z. bin Sha'ameri and F. D. B. Jaswar, "Detection of binary data for FSK digital modulation signals using spectrum estimation techniques," in *Telecommunication Technology, 2003. NCTT 2003 Proceedings. 4th National Conference on*, pp. 155-158, 2003.
- [11] B. C. Levy, *Principles of Signal Detection and Parameter Estimation*, 2008th ed. Springer, Jul. 2008.
- [12] I. Korn, "Error probability of M-ary FSK with differential phase detection in satellite mobile channel," *IEEE Trans. Vehicular Technology*, vol. 38, no. 2, Aug. 2002.

- [13] A. Arshad and S. A. Hassan, "Maximum likelihood SNR estimation for non-coherent FSK-based cooperative networks over correlated Rayleigh fading channels," *2015 IEEE Wireless Communications and Networking Conference (WCNC)*, New Orleans, LA, pp. 636-641, 2015.
- [14] W. P. Osborne and M. B. Luntz, "Coherent and Noncoherent Detection of CPFSK," *IEEE Trans. Commun.*, vol. 22, no. 8, Aug. 1974.
- [15] H. Tyagi, R. K. Mallik and S. Raina, "Optimal Receiver for MPSK Signaling with Imperfect Channel Estimation," *2007 IEEE Wireless Communications and Networking Conference*, Kowloon, 2007, pp. 483-487.
- [16] D. S. Ly-Gagnon, S. Tsukamoto, K. Katoh and K. Kikuchi, "Coherent detection of optical quadrature phase-shift keying signals with carrier phase estimation," *Journal of Lightwave Technology*, vol. 24, no. 1, pp. 12-21, Jan. 2006.